Title

A Mouse Model Suggests Two Mechanisms for Thyroid Alterations in Infantile Cystinosis: Decreased Thyroglobulin Synthesis Due to Endoplasmic Reticulum Stress/Unfolded Protein Response and Impaired Lysosomal Processing

Journal

Endocrinology, 156(6)

ISSN

0888-8809

Authors

Chevronnay, HP Gaide
Janssens, V
Van Der Smissen, P
et al.

Publication Date

2015-06-01

DOI

10.1210/en.2014-1672

Peer reviewed

A mouse model suggests two mechanisms for thyroid alterations in infantile cystinosis: decreased thyroglobulin synthesis due to endoplasmic reticulum stress/unfolded protein response and impaired lysosomal processing

H.P. Gaide Chevronnay, V. Janssens, P. Van Der Smissen, X.H. Liao, Y. Abid, N. Nevo, C. Antignac, S. Refetoff, S. Cherqui, C.E. Pierreux*, P.J. Courtoy* (*, equal last authors)

Cell Biology Unit, de Duve Institute & Université catholique de Louvain, Brussels, Belgium (H.P.G.C., V.J., P.V.D.S., Y.A., C.E.P., P.J.C.); Department of Medicine (X.H.L., S.R.), Pediatrics and Genetics (S.R), The University of Chicago, Chicago, IL, USA; Inserm, U1163, Hôpital Necker-Enfants Malades & Université Paris Descartes, Sorbonne Paris Cité, Institut Imagine, Paris, France (N.N., C.A.); Department of Pediatrics, Division of Genetics, University of California San Diego, CA, USA (S.C.)

Thyroid hormones are released from thyroglobulin (Tg) in lysosomes, which is impaired in infantile/nephropathic cystinosis. Cystinosis is a lysosomal cystine storage disease due to defective cystine exporter, cystinosin (CTNS). Cystinotic children develop subclinical then overt hypothyroidism. Why hypothyroidism is the most frequent and earliest endocrine complication of cystinosis is unknown. We here defined early alterations in *Ctns*$^{-/-}$ mice thyroid and identified subcellular and molecular mechanisms. At 9 months, T_4 and T_3 plasma levels were normal and TSH was moderately increased (~4-fold). By histology, hyperplasia and hypertrophy of most follicles preceded colloid exhaustion. Increased immunolabelling for thyrocyte proliferation and apoptotic shedding indicated accelerated cell turnover. Electron microscopy revealed endoplasmic reticulum (ER) dilation, apical lamellipodia indicating macropinocytic colloid uptake, and lysosomal cystine crystals. Tg accumulation in dilated ER contrasted with mRNA down-regulation. Increased expression of ER chaperones, GRP78 and PDI, associated with alternative XBP-1 splicing, revealed unfolded protein response (UPR) activation by ER stress. Decreased Tg mRNA and ER stress suggested reduced Tg synthesis. Coordinated increase of UPR markers, ATF-4 and CHOP, linked ER stress to apoptosis. Hormonogenic cathepsins were not altered, but LAMP-1 immunolabelling disclosed enlarged vesicles containing iodo-Tg and impaired lysosomal fusion. Isopycnic fractionation showed iodo-Tg accumulation in denser lysosomes, suggesting defective lysosomal processing and hormone release. In conclusion, *Ctns*$^{-/-}$ mice show (i) compensated primary hypothyroidism and accelerated thyrocyte turnover; (ii) impaired Tg production linked to ER stress/UPR response; and (iii) altered endolysosomal trafficking and iodo-Tg processing. The *Ctns*$^{-/-}$ thyroid is useful to study disease progression and evaluate novel therapies.

The function of individual molecular events in the thyroid gland has been unraveled by the study of monogenic defects, occurring spontaneously in human or engineered in mice (for reviews (1, 2)). We here address the effects in mouse thyroid of genetic ablation of the lysosomal membrane cystine exporter, cystinosin, which is absent in a rare multisystemic autosomal recessive lysosomal cystine storage disease, named infantile cystinosis (in short "cystinosis") (for reviews see (3, 4)). Cystinosis leads almost invariably to primary hypothyroidism during

ISSN Print 0013-7227 ISSN Online 1945-7170
Printed in U.S.A.

Received August 11, 2014. Accepted March 23, 2015.

Abbreviations:

the first years of life while other endocrine organs are later affected (4–6).

Cystinosin, a 7-transmembrane protein of 367-aa displaying two strong lysosomal targeting motives (7) is the only known lysosomal membrane cystine exporter, driven by coupled proton efflux (8). Cystine is an obligatory end-degradation product of disulfide-bearing proteins. Once exported out of lysosomes, cystine is rapidly reduced into cysteine by cytosolic reducing systems. Cysteine together with glutamate participates in glutathione synthesis, thus cell redox homeostasis. The accumulation of lysosomal cystine in cystinosis can be corrected by substrate depletion therapy based on oral cysteamine but compliance is very demanding. Cysteamine rearranges in lysosomes with cystine to a mixed disulfide that egresses via the lysine transporter (9).

The earliest manifestation of cystinosis, usually during the first year of life, is a kidney Fanconi syndrome, recognized by high urinary loss of solutes including water, salts, glucose and phosphate, together with ultrafiltrated plasma proteins. Infantile cystinosis usually leads to renal failure, even under compliant cysteamine treatment. During the first decade of life, most cystinotic children further develop subclinical then overt hypothyroidism (5, 10). Although early compliant cysteamine treatment improves body growth and can avoid thyroid hormone replacement (11), eventually about half of treated cystinotic adults require thyroid hormones. Overall, kidney and thyroid dysfunctions are the less cysteamine-preventable complications of cystinosis (12, 13). Thus, better understanding of cellular and tissular pathogenic mechanisms in kidneys and thyroid are mandatory.

The exact causative link between cystinosis and hypothyroidism remains unexplained. As for kidneys, defective thyroid function was originally attributed to atrophy with pathognomonic cystine crystals (5). However, the pathogenic role of crystals is questioned and early impairment of proteolysis in cystinotic lysosomes has been evidenced and attributed to lysosomal redox imbalance (14). Thyroid hormones (TH) are released in lysosomes by proteolytic cleavage of engulfed thyroglobulin (Tg), although proteolysis may be initiated in the follicular lumen (15, 16). Tg is an oligomer of 330 kDa monomers which assume a compact globular form stabilized by a huge number of disulfide bonds (> 100/monomer) (17). Tg is dimerized in the ER then undergoes compaction in the follicular lumen by intermolecular disulfide cross-linking, to form insoluble thyroid globules for maximal storage (18, 19). Luminal compaction is attributed to extrinsic (secreted PDI) and intrinsic disulfide bond exchange mechanisms (via well-preserved thioredoxin (CXXC) motives) (20). The extent of luminal Tg cross-linking varies among species and is related to age and follicle activation state (18, 19, 21). Tg unfolding via disulfide bond reduction by lysosomal reducing equivalents thus appears necessary to expose cryptic peptides targeted by lysosomal proteases (22). Stepwise Tg proteolytic processing depends on synergistic endo- then exopeptidases, including the aspartyl protease, cathepsin D, and cysteine proteases, a.o. cathepsin B, (23–27). Cysteine proteases also require a reducing environment. These requirements seem to predict that Tg unfolding and cysteine protease attack are impaired when lysosomal cystine accumulation causes redox imbalance.

At low TSH, basal TH production is supported by endocytosis of Tg from the colloid via small endocytic pits (ie, micropinocytosis, reviewed in (28)). This is regulated by expression and activation of tandem rate-limiting GTPase catalysts, Rab5 and Rab7, driving together vesicular transfer to lysosomes (29, 30). In some species such as mice, acute stimulation with high TSH dose triggers micrometric colloid uptake by protrusion of actin-dependent lamellipodia followed by macropinocytosis (also named phagocytosis; (31)), which brings large amounts of Tg to lysosomes in the form of "colloid droplets". How released TH cross the lysosomal membrane remains unknown. This step could involve a similar transporter as monocarboxylate transporter-8 (Mct-8) (32) operating at the basolateral membrane for secretion into blood capillaries. However, a Mct-8 defect is unlikely in a monogenic disorder such as cystinosis.

We and others recently reported on the early kidney lesions and adaptations (33, 34) in a cystinosin-knockout mice strain of congenic C57BL/6 background (*Ctns*$^{-/-}$ mice), which mimics human cystinosis (35, 36). After a 3-months lag phase without detectable lesion, proximal tubular cells (PTCs) of *Ctns*$^{-/-}$ mice showed defective endolysosomal trafficking and lysosomal proteolysis resulting into amorphous lysosomal inclusions, then cystine crystals. At the lesional stage, apoptosis and proportional proliferation revealed accelerated PTC turnover (33). We here extended our study of *Ctns*$^{-/-}$ mice to the thyroid gland, on the premise of shared high apical endocytic activity of disulfide-rich proteins, and early defects in cystinotic children.

We first hypothesized that cystine accumulation in lysosomes of *Ctns*$^{-/-}$ thyrocytes would primarily affect thyroid function by delaying TH generation, due to impaired Tg transfer to lysosomes, combined with defective unfolding and cysteine protease activity. As an additional hypothesis, nonmutually exclusive upstream mechanism, cystinosis causes endoplasmic reticulum (ER) stress (37) to which thyrocytes are particularly prone (38), so that ER stress would impair Tg synthesis, and its supply to lysosomes. ER stress triggers the complex adaptive unfolded

Antibody Table.

Peptide/protein target	Antigen sequence (if known)	Name of Antibody	Manufacturer, catalog #, and/or, name of individual providing the antibody	Species raised in; monoclonal or polyclonal	Dilution used
E-cadherin	-	Purified Mouse Anti-E-cadherin	DB Bioscience, #610 182	mouse monoclonal (clone 36)	0,25 μg/ml
Ki67	-	Purified Mouse Anti-Human Ki-67	DB Pharmingen, #556 003	mouse monoclonal (clone B56)	2 μg/ml
active-caspase 3	-	Cleaved Capsase-3 (Asp175) Antibody	Cell Signaling, #9661	rabbit polyclonal	1/200
PECAM-1	-	Rat monoclonal anti-mouse endothelial cell marker CD31 (PECAM-1)	Dianova, #DIA310	rat monoclonal (clone SZ31)	1/20
Ezrin	aa 362–585	Ezrin/p81/80K/Cytovillin Ab-1, Mouse Monoclonal Antibody	Thermo Scientific, #MS-661-P1	mouse monoclonal (clone 3C12)	2 μg/ml
LAMP-1	-	Anti-LAMP-11 1D4B Antibody	Hybridoma Bank, #1D4B	rat monoclonal (clone 1D4B)	1/100
KDEL	-	Anti-KDEL [MAC256] Antibody	Abcam, #ab50601	rat monoclonal (clone MAC256)	1/300
Thyroglobulin	-	Monoclonal Mouse Anti-Human Thyroglobulin	Dako, #M0781	mouse monoclonal (clone DAK-Tg6)	1/200; 1/1000
Iodo-thyrogobulin	-	Anti-Iodo-Thyroglobulin Antibody	provided by Dr Ris-Stalpers	mouse monoclonal	1/100; 1/1000
GRP78	CT(643)GEEDTSEKDEL(654)	GRP78/BiP Antibody	Thermo Scientific, #PAI-014A	rabbit polyclonal	2 μg/ml
Cathepsin D	-	cathepsin D Antibody	Santa Cruz, #sc-6486	goat polyclonal	0,2 μg/ml
GAPDH		GAPDH Antibody	Ambion, #AM4300	mouse monoclonal (clone 6C5)	05 μg/ml

protein response (UPR) (for review see (39)). UPR is initiated by transmembrane ER sensors/receptors, inositol-requiring kinase 1 (IRE1), protein kinase RNA-like endoplasmic reticulum kinase (PERK) and/or activating transcription factor 6 (ATF-6). IRE1 activation results from high substrate competition, causing dissociation of ER resident chaperones such as glucose-regulated protein 78kD (GRP78). Downstream in the UPR pathway, activation of X-box binding protein-1 (XBP-1) by alternative mRNA splicing results into multiple structural and molecular adaptive mechanisms. These include (i) expansion of ER membrane, thus ER dilatation to accommodate protein overload; (ii) increased transcription of ER chaperones (GRP78), and foldases (eg, protein disulfide isomerase; PDI), thus protein maturation capacity; and (iii) decreased translation of secreted proteins (here Tg), which together attenuate ER stress. If stress persists or adaptive response fails, cell death is triggered via transcriptional activation of proapoptotic C/EBP homologous protein (CHOP) in response to PERK-ATF-4 axis activation (for reviews, see (39, 40)).

We found that, after a lag phase of ~6 months, all *Ctns*$^{-/-}$ mice developed subclinical hypothyroidism with increased TSH, thyrocyte hyperplasia/hypertrophy and accelerated turnover as well as angio-proliferative response. Relative TSH refractoriness and colloid exhaustion could be explained by the combination of impaired Tg production due to UPR response with defective endolysosomal trafficking and Tg processing. UPR response to ER stress likely links TSH stimulation to thyrocyte apoptosis and accelerated turnover.

Materials and Methods

Mice

Congenic C57BL/6 *Ctns*$^{-/-}$ mice have been described (36). Mice were treated according to the NIH Guide for Care and Use of Laboratory Animals. Mice were fed ad libitum with pellets containing 4.30 mg/kg iodine (Carfil Quality).

TSH, T_4 and T_3 plasma concentrations

Plasma TSH concentrations were measured by a sensitive, heterologous, disequilibrium double-antibody precipitation RIA as described (41). T_4 and T_3 concentrations were measured by coated-tube RIA (Siemens Medical Solution Diagnostics, Los Angeles, CA).

Histology, multiplex immunofluorescence and morphometry

Mice thyroids were fixed in situ by whole-body perfusion-fixation as described (33). Thyroids were dissected, postfixed overnight with 4% neutral-buffered formaldehyde (4%F) and processed for paraffin embedding. Four μm-thick sections were stained with hematoxylin/ eosin. Immunofluorescence was performed after antigen retrieval as described (33). Appropriate combinations of the following primary antibodies were used: mouse anti-E-cadherin (0.25 μg/ml; DB Bioscience, 610 182), -ezrin (2 μg/ml; Thermo Scientific, #MS-661-P1), -Ki67 (2 μg/ml; DB Pharmingen, #556003), -Tg (1/200; Dako, #M0781) and -iodo-Tg (1/100; kindly donated by Dr. Ris-Stalpers, Laboratory of Pediatric Endocrinology, Academic Medical Center, Amsterdam, Netherlands), rat anti-PECAM-1 (1/20; Dianova, #DIA310), -LAMP-1 (1/100; Hybridoma Bank, #1D4B), and -KDEL (1/300; Abcam, #ab50601); and rabbit antiactive caspase 3 (1/200; Cell Signaling, #9661). Immunolabeled sections were imaged with a spinning disk confocal microscope using EC Plan-NeoFluar 40X/1.3 or Plan Apochromat 100x/1.4 Oil DIC objectives (Cell Observer Spinning Disk; Zeiss, Oberkochen, Germany). Morphometric analyses were performed using Axiovision 4.8.2. Software (Zeiss). Binary mask were prepared using fixed interactive thresholding. Thyrocytes, colloid and interstitium were filled and areas were measured.

Electron microscopy

Thyroids were perfusion-fixed in situ with 4% F supplemented by 0.1% glutaraldehyde; then immersion-fixed in 1.5% (v/v) glutaraldehyde overnight, postfixed with 1% (w/v) OsO_4 in 0.1M cacodylate buffer for 1h, rinsed in veronal buffer (4 × 5min) and stained overnight "en bloc" in 1% neutral uranyl acetate, all at 4°C. After extensive washing in veronal, blocks were dehydrated in graded ethanol and embedded in Spurr. Ultrathin sections were obtained (Reichert ultramicrotome), collected on 400-mesh rhodanium grids and contrasted with 3% uranyl acetate then lead citrate, 10 minutes each. Grids were washed with water, dried, and examined in a FEI CM12 electron microscope (EM) operating at 80 kV.

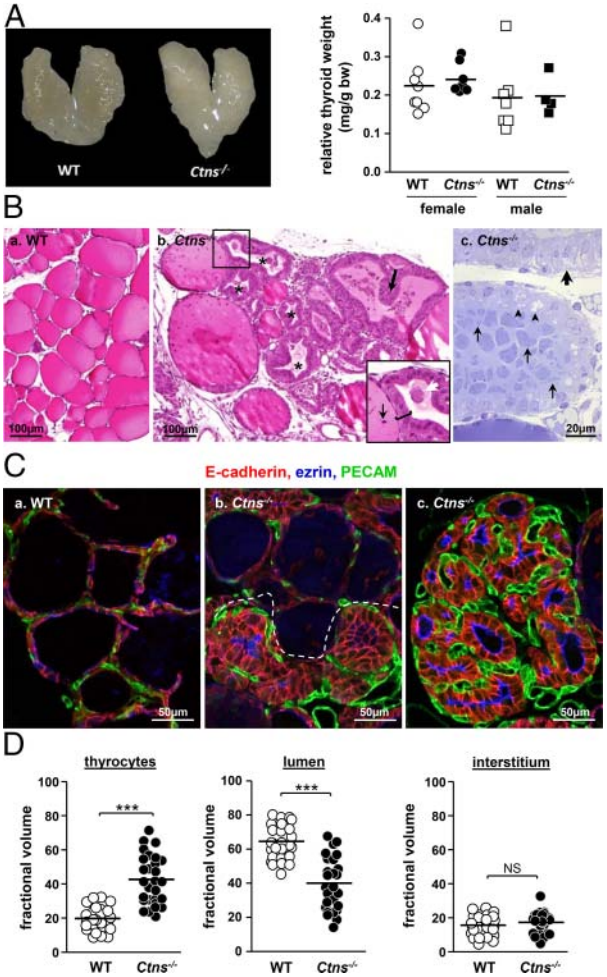

Figure 1. *Ctns*$^{-/-}$ mice develop thyroid hyperplasia and hypertrophy associated with colloid exhaustion. **A. Anatomy.** Left: Thyroid gland from control (WT) and *Ctns*$^{-/-}$ female mice at 11 months. Right: Thyroid glands weight normalized to body weight in WT and *Ctns*$^{-/-}$ female and male at 9–12 months. Cystinotic mice do not develop goiter. **B. Histology.** (a,b) Paraffin sections with hematoxylin-eosin staining and (c) semithin plastic section with toluidine blue staining (c), all at 9 months. **(a)** WT thyroid is made of uniform follicles filled with homogenous colloid and delimited by flat thyrocytes. **(b)** In *Ctns*$^{-/-}$ mice, most follicles show exhausted colloid (asterisks) surrounded by thyrocytes that are both hypertrophic (insert bracket) and hyperplastic, frequently projecting into papillae (thick arrow). Boxed area at b is enlarged below to emphasize the contrast between the few resting follicles (flat epithelium) with colloid bearing several cell remnants (thin arrow) and an adjacent hypertrophic/hyperplastic follicle (bracket) with almost vanished colloid (white arrow suggests dissolution of a thyroid globule). **(c)** In the plastic section of *Ctns*$^{-/-}$ thyroid, the two upper follicles with hypertrophic thyrocytes and exhausted colloid contrast with a resting follicle below with dense colloid and flat thyrocytes. Arrowheads point to apical thyrocyte vacuolation, suggesting macropinocytosis/phagocytosis; the thick arrow points to irregular basal thyrocyte clarifications aligned along the baso-apical axis, suggesting dilation of endoplasmic reticulum. In the central follicle, shed cell remnants almost fill the follicular lumen (thin arrows indicate variety of shapes). Scale bars, 100 μm. *For histological time-course, see Suppl Figure 1.* **C, D. Immunofluorescence: multifocal activation of the angio-follicular system in *Ctns*$^{-/-}$ mice thyroids and colloid exhaustion. C. Follicular hyperplasia and hypertrophy are coupled to expansion of associated blood capillary basket.** Multiplex immunofluorescence for E-cadherin (red, thyrocyte baso-lateral membrane), ezrin (blue, thyrocyte apical membrane) and PECAM (green, blood capillaries) in the thyroid of WT (a) and *Ctns*$^{-/-}$ (b-c) mice at 9 months, performed strictly in parallel. **(a)** WT follicles are surrounded by a blood capillary network weakly discernible by PECAM immunolabeling. **(b)** In this intermediate *Ctns*$^{-/-}$ pattern, notice abrupt boundary (dotted line) between resting follicles (top) and hyperplastic follicles (bottom) showing microvasculature expansion associated with much stronger PECAM signal. (**c**) In most remodeled *Ctns*$^{-/-}$ hyperplastic foci, lumina have almost vanished and microvasculature is greatly expanded. All scale bars, 50 μm. *For in situ hybridization of Vegf-a, see Suppl Figure 2.* **D. Follicular hyperplasia/hypertrophy is associated with colloid exhaustion**. Morphometric assessment of the fractional volume of thyrocytes, colloid and interstitial compartment (mesenchyme and blood capillaries) in WT and *Ctns*$^{-/-}$ mice (n = 3; each analyzed in 9 random fields spanning the entire thyroid section, cumulative area of 3.4 10^5 μm^2 for each mice). Note doubling of *Ctns*$^{-/-}$ thyrocyte fractional volume, at the expense of the lumen, but no significant change of interstitial fractional volume. ***$P < .001$; NS, not significant.

In situ Hybridization

Vegf-a antisense RNA probes spanning nucleotides 94 to 429 of the mouse coding sequence for Vegfa (42) were produced by RT-PCR followed by in vitro transcription with T7 RNA polymerase in presence of digoxigenin-labeled uridine 5-triphosphate (Roche). In situ hybridization was performed on 8-μm sections as described (33).

PCR and RT-qPCR

Total RNA was extracted (TRIzol® Reagent; Invitrogen) and 150ng RNA were reverse-transcribed by M-MLV reverse transcriptase (Invitrogen) using random hexamers. Primer sequences are described in Supplemental Table 1. PCR was performed under standard conditions with GoTaq® DNA Polymerase (Promega). Real-time qPCR was performed as described (33) in presence of 250 nM specific primers with Kappa SYBR Fast qPCR Master Mix (Kapa Biosystems) on a CFX96 touch real-time PCR Detection System (Bio-Rad). Results are presented as difference of cycle threshold (ΔCt) values normalized to actin, used as internal standard.

Western and Lectin Blotting

Thyroid glands were dissected and homogenized in RIPA buffer (150 mM NaCl, 1% TritonX-100, 0.5% sodium deoxycholate; 0.1% SDS, 50 mM Tris, pH8.0) or in 250 mM sucrose, 3 mM imidazole and 1 mM EDTA pH7.0 buffer supplemented with Complete Protease Inhibitors (Roche) and phosphatase inhibitors (sodium orthovanadate, pyrophosphate and fluoride, all 2 mM). Loading was normalized to protein concentration, measured by bicinchoninic acid method (Sigma-Aldrich). Samples were reduced or not, as indicated, with 50 or 100 mM DTT for 10 minutes and denatured by boiling for 5 minutes. Western blotting were performed as described (43) using mouse anti-Tg (1/1000, Dako, #M0781), or -glyceraldehyde-3 phosphate deshydrogenase (GAPDH; 0.5 μg/ml, Ambion, #AM4300); rat anti-KDEL (2.5 μg/ml, Abcam, #ab50601); rabbit anti-GRP78 (2 μg/ml, Thermo Scientific, #PA1–014A); or goat anticathespin D (0.2 μg/ml, Santa Cruz, #sc-6486). Lectin blotting was performed with wheat germ agglutinin lectin (10 μg/ml, Vector Bio-

lab) after electrophoresis under reducing conditions as described (44). Specificity of lectin signal was demonstrated by neuraminidase digestion at 37°C for 18h, following manufacturer's instructions (New England BioLabs).

Cathepsin B Assay

Thyroid glands were dissected and homogenized in 250 mM sucrose, 3 mM imidazole and 1 mM EDTA, pH7.0. Cathepsin B activity was measured by total minus 100 μM CA-074-resistant fraction (Sigma-Aldrich), after fluorimetric assay using benzyloxycarbonyl-L-phenylalanyl-L-arginine 4-methylcoumaryl-7-amide (Z-Phe-Arg-AMC) (45), or Nα-benzoyl-$_{DL}$-arginine-β-naphthylamide hydrochloride (BANA), with undistinguishable results. Activity was normalized to protein concentration measured by bicinchoninic acid method (Sigma-Aldrich).

Analytical Subcellular Fractionation

Excised thyroid glands from 3 to 4 WT or *Ctns*$^{-/-}$ mice, aged 9–11 months, were pooled in 250 mM sucrose, 3 mM imidazole and 1 mM EDTA, pH7.0, supplemented with Complete Protease Inhibitors, and homogenized therein with a Polytron (3 × 5 seconds, #8500 speed). Homogenates were cleared through 40 μm BD falcon filters and first resolved by crude differential sedimentation to isolate cell debris and nuclei (1.5 10^4 *g* x min), postnuclear particles (6.3 10^6 *g* x min) and a final supernatant. Postnuclear particles were washed once by resuspension and resedimentation to minimize colloid contamination, then equilibrated by sedimentation into 1.10–1.30 (g/ml) linear sucrose gradients in a SW55Ti rotor (57 10^6 *g* x min). Ten fractions were collected from the bottom and assayed for density (weight) and β-hexosaminidase activity as described (33). Aliquots of equal volume were analyzed by western blotting for iodo-Tg (1/1000). Compared blots were transferred and revealed in the same membrane then quantified using ImageJ.

Statistical analyses

Statistical significance was tested using Mann-Whitney test (Figure 1A, Figure 3A-B, Figure 5B, Figure 6C, Figure 7B-C; Suppl Figure 4), Student's *t* test (Figure 1D, Figure 2B) or Chi2 (Figure 6B). Differences were considered significant for $P < .05$.

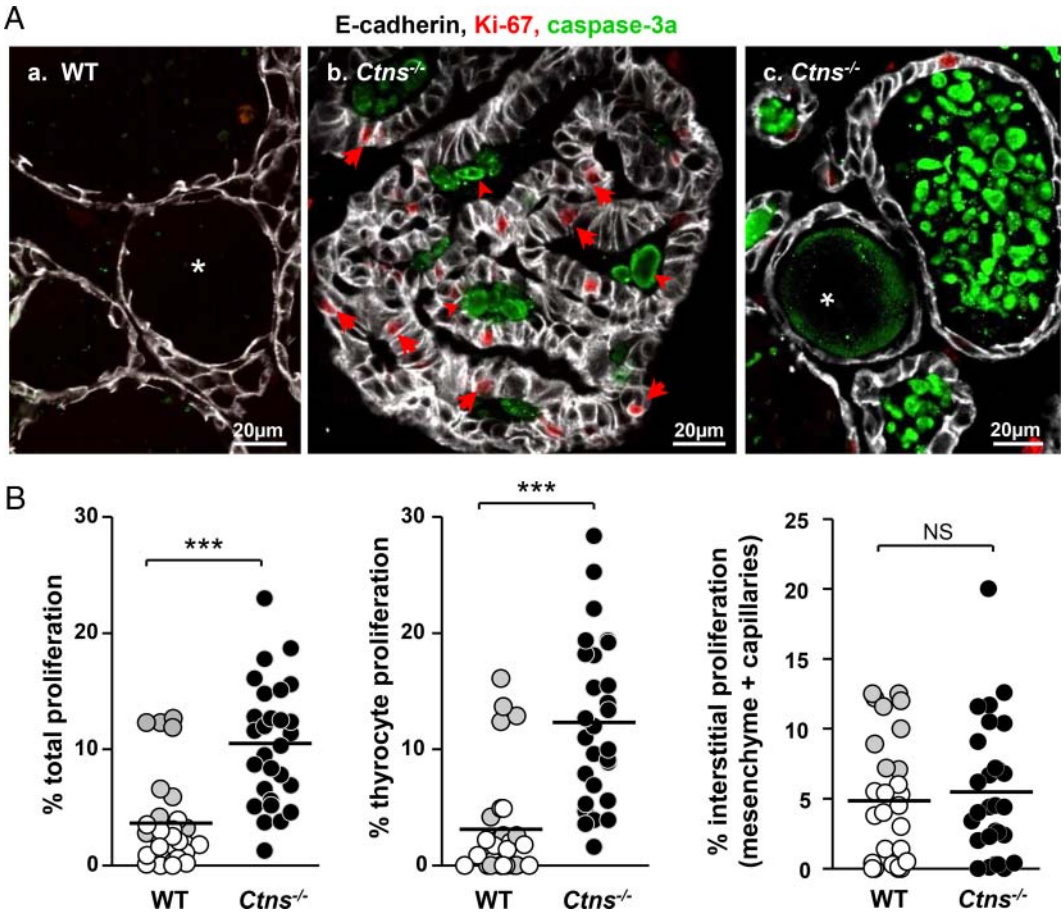

Figure 2. Cystinosis induces follicle-autonomous thyrocyte proliferation and apoptosis. A. Confocal microscopy. Immunofluorescence for E-cadherin (white; thyrocyte baso-lateral membrane), Ki-67 (red; cell proliferation marker) and activated caspase-3 (green, apoptosis marker) in 9 months WT **(a)** and *Ctns*$^{-/-}$ **(b)** thyroids. Notice numerous proliferating cells (arrows) in *Ctns*$^{-/-}$ hyperplastic follicles, pointing to autonomous follicular response, whereas Ki-67 labeling in WT thyrocytes is very rare. At **(c),** large collections of apoptotic bodies in the follicular lumen of *Ctns*$^{-/-}$ thyroid (arrowheads) indicate accelerated cell turn-over. All scale bars, 20 μm. **B. Quantification of proliferation**. Percentage of total nuclei area stained for Ki-67 in whole tissue (total proliferation) or associated to E-cadherin (thyrocyte proliferation) as estimated by morphometric analysis in 9 months WT (open and gray symbols; gray identifies a special WT individual) and *Ctns*$^{-/-}$ thyroids (filled symbols) (n = 3). For each mice, 3.4 10^5 μm^2 of area corresponding to 9 fields spanning the entire thyroid section were analyzed. Proliferation is specifically increased in *Ctns*$^{-/-}$ thyrocytes; ***$P < .001$.

Except for specific thyroid weight, there was no significant difference between males and females in each group and for each comparison, thus genders were not discriminated on scatter plots.

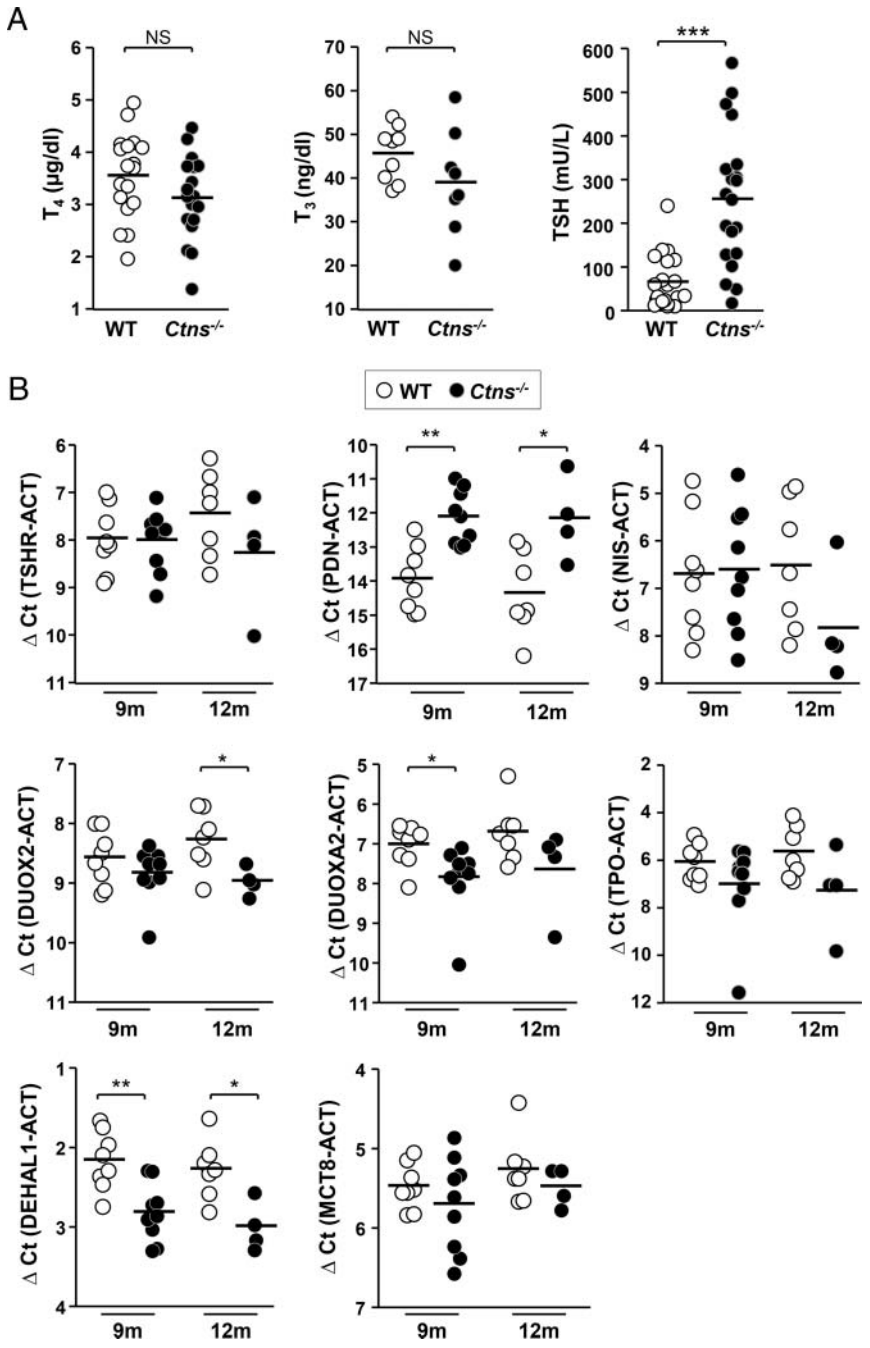

Figure 3. Compensated primary hypothyroidism and mRNA expression of thyroid hormone synthesis machinery in *Ctns*$^{-/-}$ mice. A. *Ctns*$^{-/-}$ mice elicit a compensatory TSH increase. T_4, T_3 and TSH plasma concentrations were measured in 9–10 months WT mice (open symbols) and *Ctns*$^{-/-}$ littermates (filled symbols) (n = 18 for T_4; 9–8 for T3; 20 for TSH). *Ctns*$^{-/-}$ mice show an average 4-fold increase in plasma TSH level but still normal thyroid hormone plasma levels, indicating effective thyroid compensation. **B Expression of thyroid-specific gene involved in hormone synthesis.** Quantification by RT-qPCR of TSH receptor (TSHR), Na/I symporter (NIS), pendrin (PDN), dual oxidase 2 (DUOX2), dual oxidase maturation factor 2 (DUOXA2), thyroperoxidase (TPO), iodotyrosine dehalogenase 1 (DEHAL1) and monocarboxylate transporter 8 (MCT8) mRNAs in WT and *Ctns*$^{-/-}$ thyroids collected at 9 and 12 months, normalized to actin (ACT) and presented as ΔCt values (difference of cycle threshold).

Results

Ctns$^{-/-}$ thyroids develop multifocal hyperplasia/hypertrophy with colloid exhaustion and proportional vascular expansion

There was neither macroscopic change nor goiter at 9 and 12 months (Figure 1A). Thyroid glands were analyzed by conventional histopathology at 3, 6, 9, and 15 months (Figure 1B and Suppl Figure 1). There were no detectable lesions at 3 months. Between 6 and 9 months, *Ctns*$^{-/-}$ mice consistently developed multifocal thyrocyte hypertrophy and hyperplasia with pseudostratification up to papillary lesions, luminal cell remnants (Fig 1Bb, c) and colloid exhaustion (Fig 1Bb). As better seen with 1-μm plastic sections, hypertrophic thyrocytes exhibited apical vacuolation, suggesting (TSH)-induced macropinocytosis/phagocytosis, and irregular basal cytoplasm clarification, suggesting endoplasmic reticulum (ER) dilatation (Fig 1Bc). As disease progressed, luminal cell remnants accumulated (Fig 1Bc) and colloid vanished (Suppl Figure 1). At 15 months, most *Ctns*$^{-/-}$ follicles were hyperplastic or dedifferentiated, with few resting follicles remaining visible. In 15-months wild-type (WT) thyroids, most follicles remained quiescent and few peripheral follicles were activated. To focus on consistent early physiopathological mechanisms, mice were further analyzed at ~9 months.

The importance of thyroid capillaries as integrated part of autonomous angio-follicular units has emerged (46). Since blood capillaries are barely visible by conventional histology, we looked for vascular changes by triple immunofluores-

cence confocal imaging, using E-cadherin and ezrin as markers of thyrocyte membrane domains, together with PECAM for blood capillaries. *Ctns*$^{-/-}$ hyperplastic follicles were consistently associated with prominent dilated capillaries as compared to resting follicles, indicating synchronous activation of the angio-follicular system (Figure 1C). Proangiogenic Vegf-a was up-regulated in hypertrophic thyrocytes, mostly in papillary projections, in full agreement with recruitment/expansion of blood capillaries (Suppl Figure 2). Thus, *Ctns*$^{-/-}$ mice exhibited integrated angio-follicular activation.

To quantitate tissue changes by taking into account disease-induced heterogeneity between mice and between follicles, we exploited E-cadherin immunofluorescence (Figure 1D). Thyrocyte fractional volume was increased by 2.2-fold in *Ctns*$^{-/-}$ mice (19.9% in WT vs 42.9% in *Ctns*$^{-/-}$ mice) with a concomitant decrease of fractional luminal volume (64.5% in WT vs 39.9% in *Ctns*$^{-/-}$ mice). Both parameters showed strong negative correlation ($r = 0.93$; $P < .0001$; not illustrated). No significant difference was observed between WT and *Ctns*$^{-/-}$ mice for interstitial area (combined mesenchyme and blood capillaries). We thus focused on thyrocytes for further structural studies.

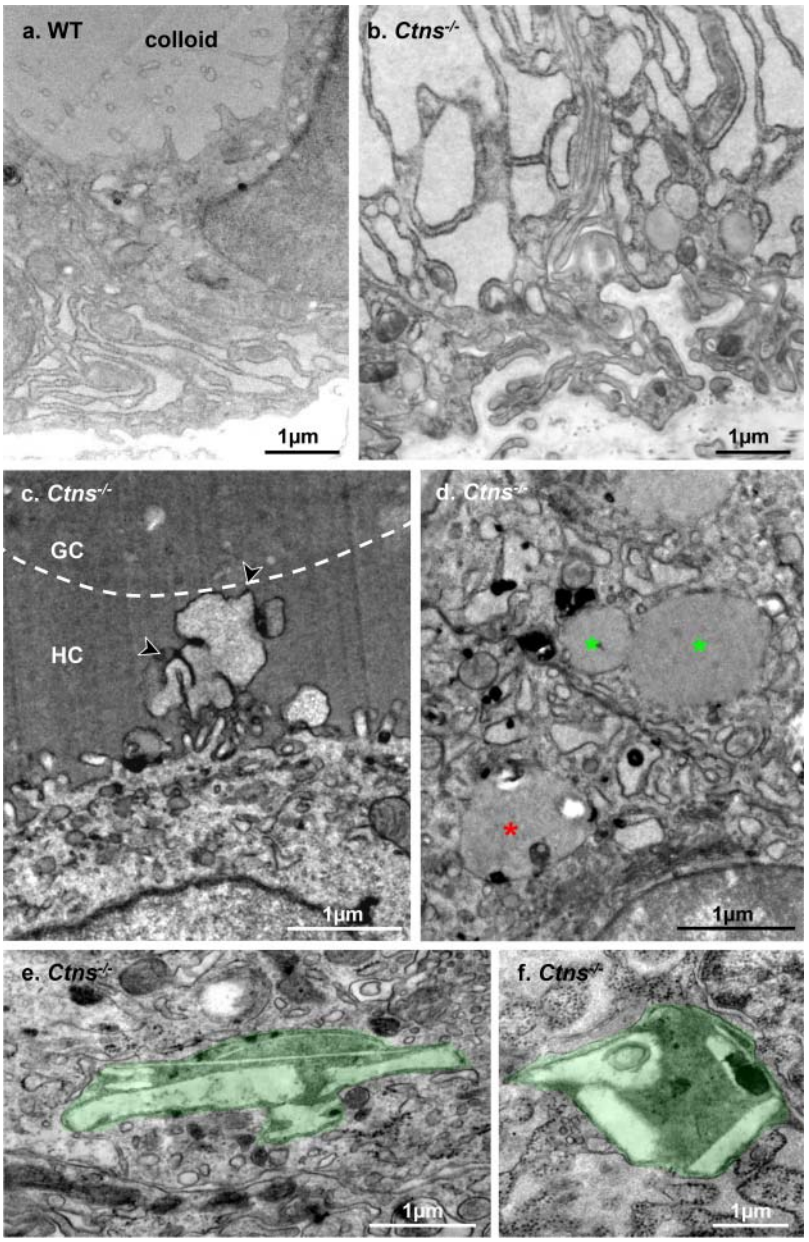

Figure 4. Ultrastructural alterations in *Ctns*$^{-/-}$ thyrocytes. Representative EM views of resting WT (a) and activated *Ctns*$^{-/-}$ thyrocytes (b-f). **(a)** In this resting WT thyrocyte at 12 months, notice limited ER expansion and thin apical projections. **(b)** Hyperplastic *Ctns*$^{-/-}$ thyrocyte at 12 months showing strong dilatation of endoplasmic reticulum lumen. Notice characteristic tortuous basal plasma membrane and basal lamina. **(c)** This activated *Ctns*$^{-/-}$ thyrocyte at 8 months projects a lamellipodium, characteristic of macropinocytosis (arrowheads) across an homogenous peripheral colloid ring (HC) up to central granular colloid (GC), indicated by the broken line. **(**d) Asterisks indicate colloid droplets in two adjacent activated thyrocytes, two with homogenous colloid content and undergoing homotypic fusion (green asterisks), one bearing additional luminal structures indicating fusion with lysosomes (red asterisk). **(e-f)** Cystine crystals-bearing lysosomes in *Ctns*$^{-/-}$ thyrocytes at 12 months.

Increased proliferation and apoptosis in Ctns$^{-/-}$ thyrocytes reveals accelerated cell turnover

Cell division is rare in normal adult thyrocytes (47) but was expected to increase so as to support hyperplasia in *Ctns*$^{-/-}$ thyroids. Conversely, the striking abundance of luminal remnants was reminiscent of in vitro and in vivo evidence that cystinosis triggers apoptosis in other cells/tissues (33, 48, 49). To define the impact of cystinosis on thyrocyte turnover, we analyzed proliferation and apoptosis (Figure 2A, B). Thyrocyte proliferation, monitored by Ki-67 immunolabeling, was barely detected in WT (< 3%), but significantly increased in *Ctns*$^{-/-}$ mice (by 4.5-fold). Interstitial cell proliferation did not reach significant difference between WT and *Ctns*$^{-/-}$ mice (Figure 3B, except if values of one outlier WT mouse were excluded; $P < .01$). Likewise, in WT thyroids, apoptotic events (monitored by active caspase-3 immunolabeling),

were very rare (Fig 2Aa), consistent with a resting cell population. In contrast, caspase-3a labeled apoptotic bodies accumulated in *Ctns*$^{-/-}$ follicular lumen, confirming accelerated cell turnover (Fig 2Ab,c). The distribution of apoptotic cells among follicles was much more heterogeneous than proliferative events, probably due to follicle heterogeneity in disease progression and unequal long-term retention of apoptotic bodies in follicular lumina (in contrast to continuous shedding in kidney proximal tubules; (33)).

Ctns$^{-/-}$ mice develop subclinical hypothyroidism

Because histological alterations of *Ctns*$^{-/-}$ thyroid suggested TSH activation, and since cystinotic children de-

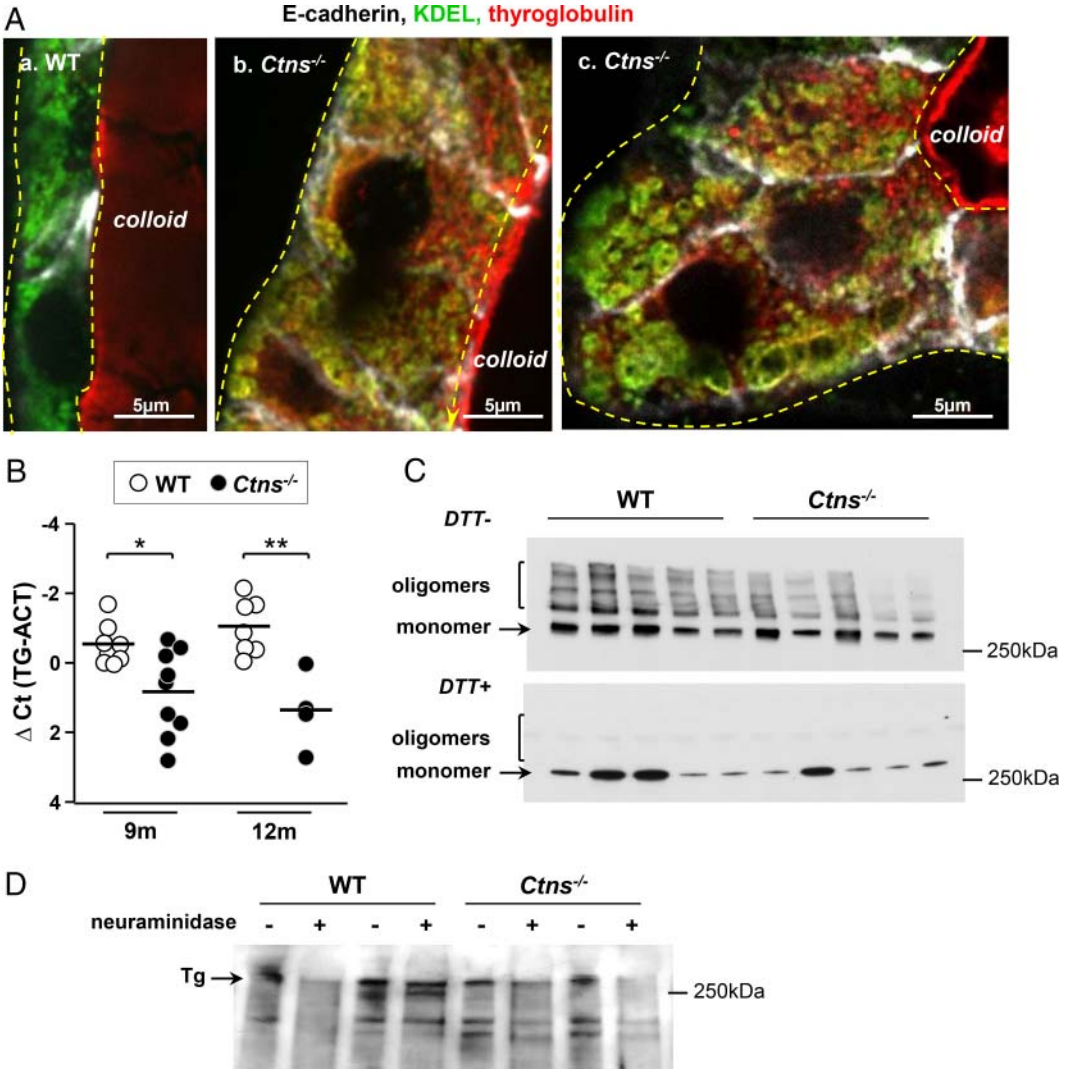

Figure 5. Tg synthesis is slowed down but maturation is qualitatively preserved in hyperplastic *Ctns*$^{-/-}$ thyrocytes. A. Tg accumulates in the endoplasmic reticulum of *Ctns*$^{-/-}$ thyrocytes. Comparison of WT **(a)** and *Ctns*$^{-/-}$ mice **(b)** at 9–10 months for E-cadherin (white), KDEL (green, retention motive used as marker of endoplasmic reticulum, ER) and Tg (red). Yellow broken lines indicate thyrocyte profiles. Tg labeling of colloid is out-of-focus, because of artifactual colloid stickiness to the coverslip. In WT thyrocytes **(a)**, the ER is usually localized to the basolateral cytoplasm (notice complementarity of green pattern with Figure 4a), without resolution of the reticulum at the confocal level, and shows barely visible Tg signal in our labeling conditions. In contrast, *Ctns*$^{-/-}$ hyperplastic thyrocytes **(b,c)** show endoplasmic reticulum dilatations, resolved at the confocal level (KDEL, green), containing detected Tg (red) resulting in yellow signal, and expanding up to the apical pole. **B. Decreased levels of Tg mRNA in *Ctns*$^{-/-}$ mice thyroid.** Quantification of thyroglobulin (TG) mRNAs by RT-qPCR in WT and *Ctns*$^{-/-}$ thyroids collected at 9 and 12 months, normalized to actin (ACT) and presented as ΔCt values. *, $P < .05$; **, $P < .01$. **C,D. Preserved thyroglobulin maturation. C, Disulfide bonding.** Thyroid extracts of 5 WT and 5 *Ctns*$^{-/-}$ thyroids were analyzed by western blotting for thyroglobulin, without or after reduction of disulfide bonds by 100 mM DTT. Notice that total Tg is decreased in *Ctns*$^{-/-}$ thyroid and that Tg oligomers remain detectable in *Ctns*$^{-/-}$ thyroids although their proportion is decreased as compared to WT. These effects are attributed to accelerated colloid turn-over. Oligomers are fully reduced into 330-kDa monomers upon DTT. Decreasing DTT concentration to 0.3 mM yielded identical results (not shown). **D, Terminal N-glycosylation.** Thyroid extracts from 2 WT and 2 *Ctns*$^{-/-}$ mice were analyzed by lectin blotting after reduction by DTT, without or with pretreatment with neuraminidase as lectin-specificity control,. Notice comparable terminal thyroglobulin sialylation. This blot is representative of 2 experiments.

velop subclinical hypothyroidism we next evaluated the thyroid hormonal status in *Ctns*$^{-/-}$ mice and analyzed the expression of critical genes involved in thyroid hormone synthesis (Figure 3B). As shown by Figure 3A, plasma TSH concentrations of *Ctns*$^{-/-}$ mice at 9–10 months were significantly increased (by 4.4-fold) as compared to WT mice, a feed-back response sufficient to maintain normal plasma T_4 and T_3 concentrations. Although mRNA of some components of thyroid hormone biosynthetic machinery were moderately altered (pendrin, DUOX2, DUOXA2, DEHAL1), none (including the basolateral transporter of TH, Mct-8) was really defective in *Ctns*$^{-/-}$ mice (Figure 3B). We concluded that *Ctns*$^{-/-}$ mice mimic subclinical hypothyroidism of cystinotic children.

Tg synthesis is quantitatively but not qualitatively altered in Ctns$^{-/-}$ mice

As an explanation for colloid exhaustion observed in *Ctns*$^{-/-}$ thyroids, we first looked at Tg biosynthetic machinery, including ER structure, disulfide-bonding and N-glycosylation. Electron microscopy revealed prominent ER dilatation in the hypertrophic *Ctns*$^{-/-}$ thyrocytes contrasting with normal Golgi complex (Figure 4a,b). Also by confocal microscopy, immunolabeling for the C-terminal endoplasmic reticulum (ER)-retention motive, KDEL, confirmed that basolateral dilations seen in semithin plastic sections of hypertrophic thyrocytes (Figure 1c) reflected a major enlargement of this compartment (Fig 5Ab,c). Simultaneous Tg immunolabeling disclosed its accumulation in the dilated ER, compatible with either increased synthesis upon TSH stimulation or defective export, eg, upon ER stress (50) (Fig 5Ab,c). To discriminate between these two hypotheses, we quantified Tg mRNA expression in thyroids at 9 and 12 months and found a significant decrease in *Ctns*$^{-/-}$ as compared to WT mice (Figure 5B). Western blotting on thyroid lysates confirmed a decreased total Tg content and revealed a decreased proportion of high-molecular weight Tg (ie, cross-linked) in *Ctns*$^{-/-}$ thyroids (Figure 5C). Irrespectively of the cystinosin status, Tg could be completely reduced by DTT into 330 kDa monomers (Figure 5C) by as low as 0.3 mM DTT (not shown). These data indicated that Tg could still oligomerize in *Ctns*$^{-/-}$ follicle lumina and suggested accelerated colloid turnover. Of note, the extent of cross-linking differed between mice studied here (low) and young human adults (higher) (21): species differences should be kept in mind when extrapolating conclusions from cystinotic mice to patients. Analysis of Tg terminal N-glycosylation by sialic acid lectin blotting of thyroid lysates revealed no major difference be-

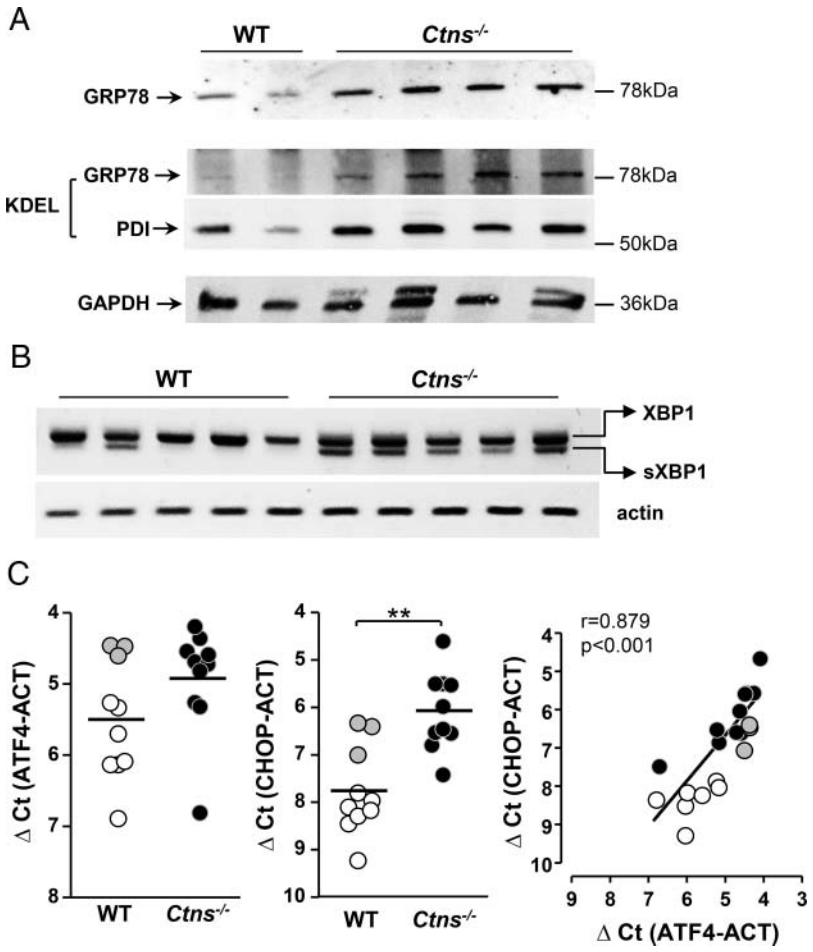

Figure 6. ER stress is triggered in *Ctns*$^{-/-}$ thyroid. A. Increased expression of GRP78 and PDI in *Ctns*$^{-/-}$ mice thyroid. Thyroid lysates from WT and *Ctns*$^{-/-}$ at 11–12 months were analyzed by western blotting with antibodies to GRP78 (upper panel) or KDEL (the latter identifies both GRP78 and PDI; medium panel) and to GAPDH (stripped reprobed blot, lower panel). **B. Unconventional splicing of XBP-1 mRNA is triggered in *Ctns*$^{-/-}$ mice thyroid**. RT-PCR analysis of XBP-1 mRNA maturation in thyroid of 5 WT and 5 *Ctns*$^{-/-}$ mice at 9 months. Notice the alternative sXBP1 lower band in all *Ctns*$^{-/-}$ samples, and only one WT sample. **C. Induction of ATF-4 expression triggers CHOP mRNA expression.** Quantification of activating transcription factor-4 (ATF-4) and C/EBP homologous protein (CHOP) mRNAs by RT-qPCR in WT and *Ctns*$^{-/-}$ thyroids collected at 9 months, normalized to actin (ACT) and presented as ΔCt values. $^{**}P < .01$. Gray dots correspond to outlier WT mice for which both ATF-4 and CHOP were increased. At right, increased expression of ATF-4 strongly correlates with increased expression of CHOP.

tween WT and *Ctns*$^{-/-}$ mice (Figure 5D). We thus concluded that Tg processing was qualitatively preserved in *Ctns*$^{-/-}$ mice and that ER enlargement was not due to increased Tg *synthesis*, pointing instead to quantitative defect in export, possibly upon ER stress.

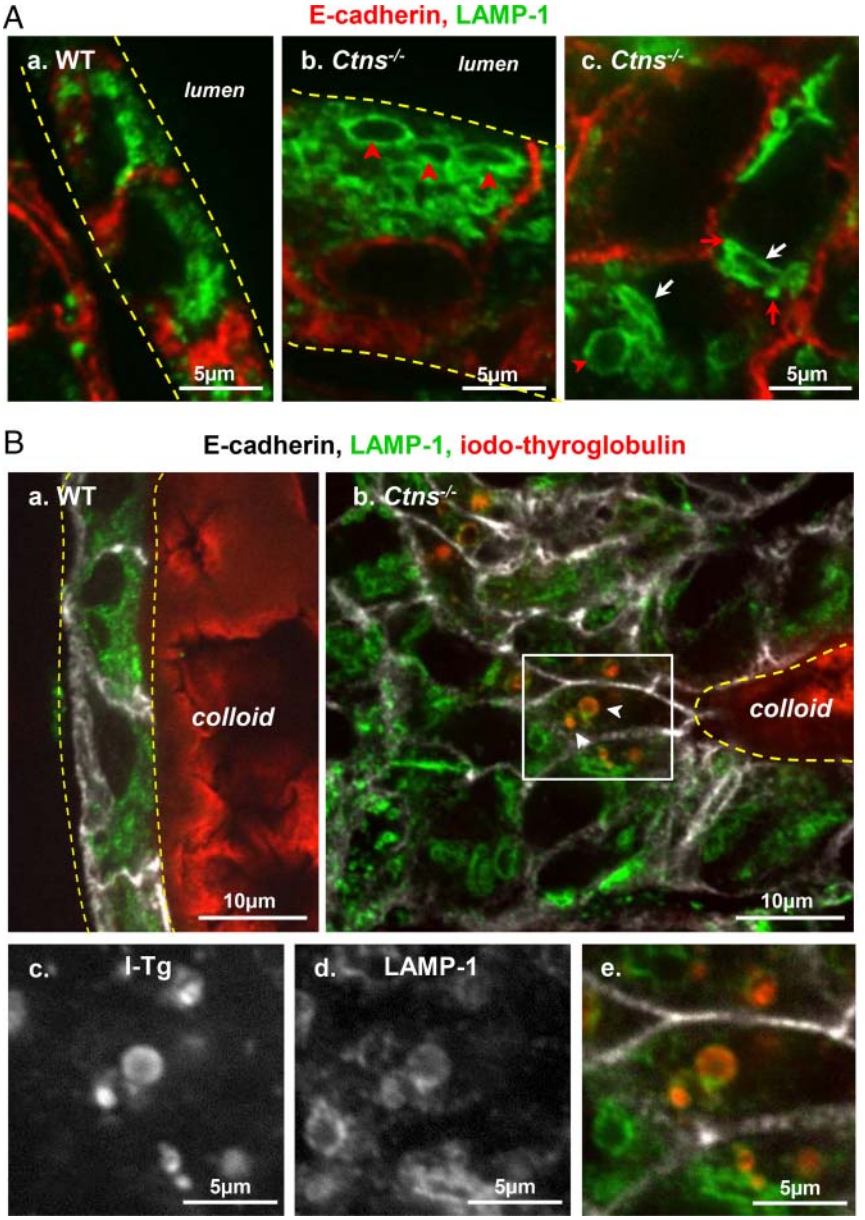

Figure 7. Alterations of the late endocytic apparatus in hyperplastic *Ctns*$^{-/-}$ thyrocytes. A. Identification of large apical vacuoles and crystal-bearing structures as lysosomes. Comparison of WT **(a)** and *Ctns*$^{-/-}$ mice **(b-c)** at 9 months for immunolabeling of E-cadherin (red) and LAMP-1 (green; late endosome/lysosome membrane). **(a)** In this resting WT follicle, flat thyrocytes show at their apical pole packed lysosomes of uniform small size and round shape. **(b-c).** In activated *Ctns*$^{-/-}$ thyrocytes, late endosomes-lysosomes are frequently dilated (red arrowheads) and distorted (better seen at c, white arrows). Red arrows at c suggests docked but not fused late endosomes/lysosomes. *For levels of Rab5 and Rab7 mRNAs, see Suppl Figure 4.* **B. Iodo-Tg is retained in lysosomes**. Comparison of WT **(a)** and *Ctns*$^{-/-}$ mice **(b-e)** at 9–10 months for E-cadherin (white), LAMP-1 (green) and iodo-Tg (red). In resting WT follicles **(a)**, iodo-Tg is stored in the colloid and is never detected within thyrocytes. In activated *Ctns*$^{-/-}$ thyrocytes **(b)**, vesicles filled with iodo-Tg and labeled by LAMP-1 (thus not primary colloid droplets) are frequently found at the apical pole of hyperplasic thyrocytes. Enlargements of the boxed field **(c-e)**, first show single-channel images of iodo-Tg and LAMP-1 in black-and-white for optimal resolution and easier pattern comparison, then merged back with E-cadherin in triple colors as above. The apparent defect of (iodo-)Tg labeling of the central lumen is due to artifactual sticking of the colloid to the coverslip, thus out-of-focus by confocal imaging. *For a gallery of representative images of iodo-Tg retained in lysosomes, see Suppl Figure 3.*

Ctns$^{-/-}$ thyrocytes develop the unfolded protein response to ER stress

Secretory cells are particularly prone to ER stress, previously documented in activated thyrocytes (38, 50). Moreover, cystinosis has been associated with ER stress (51). We thus evaluated whether the unfolded protein response (UPR) was activated in response to ER stress in *Ctns*$^{-/-}$ thyroid, by looking at UPR-target genes and products (52, 53). The ER-resident chaperone GRP78 and PDI, both bearing the KDEL ER-retention motive, were increased at the protein level in *Ctns*$^{-/-}$ thyroid homogenates (Figure 6A). Downstream in the UPR pathway, unconventional splicing of transcription factor XBP-1 mRNA, yielding the sXBP1 form, was detected in almost all *Ctns*$^{-/-}$ thyroids but only in a minority of WT thyroids. As shown by Figure 6B, at 9 months, 10/13 *Ctns*$^{-/-}$ vs 3/9 WT mice thyroids exhibited nonconventional XBP-1 mRNA splicing ($P < .001$); at 12 months, the proportion were 8/9 *Ctns*$^{-/-}$ vs 2/8 WT ($P < .01$; not shown). Further in the UPR pathway, induction of ATF-4 expression strongly correlated with increased expression of its downstream effector, the transcription factor CHOP (Figure 6C). These data together supported the hypothesis that activation of ER stress/UPR pathway in *Ctns*$^{-/-}$ thyrocytes not only leads to defective Tg synthesis and secretion, thus colloid exhaustion, but also contributes to apoptosis triggering.

Lysosomal Tg processing is altered in Ctns$^{-/-}$ mice

Besides UPR effects, our alternative working hypothesis for primary hypothyroidism was defective release of thyroid hormones from iodo-Tg. To this aim; we looked for ultrastructural alterations of the endocytic apparatus (Figure 4) and at LAMP-1 immunofluorescence for late endosomes/lysosomes (Figure 7). By electron microscopy (EM), while apical surface of resting WT thyrocytes only showed sparse thin microvilli (Figure 4a), *Ctns*$^{-/-}$ thyrocytes in activated follicles frequently showed apical lamellipodia (Figure 4c), sequestration of primary colloid droplets and their fusion into phagolysosomes (Figure 4d). These are characteristic of TSH-induced macropinocytosis, the structural equivalent of accelerated endocytosis. In contrast, we detected no change in the abundance of Rab5 and Rab7mRNAs which finely tune micropinocytosis (Suppl Figure 4). By immunofluorescence, induced macropinocytosis correlated with enlarged LAMP-1-labeled apical structures (Fig 7Ab), absent in resting WT thyrocytes (Fig 7Aa). In addition, LAMP-1 labeled some distorted structures (Fig 7Ac), either strongly elongated or showing angular membranes, reminiscent of the abundant lysosome-bearing crystals in *Ctns*$^{-/-}$ kidney proximal tubular cells (33). Electron microscopy of *Ctns*$^{-/-}$ thyrocytes yielded several examples of severely physically disabled secondary lysosomes, identified by a limiting membrane and heterogeneous content, and containing characteristic electron-lucent needles or long polyhedric objects, ie, *bona fide* cystine crystals (Figure 4e,f). Remarkably, small LAMP-1-labeled vesicles appeared closely apposed to distorted LAMP-1-labeled structures, suggesting lysosomal docking but impaired fusion (Fig 7Ac) as seen in *Ctns*$^{-/-}$ PTCs where a late endocytic trafficking defect has been evidenced.

Since late endocytic trafficking seemed affected in *Ctns*$^{-/-}$ thyrocytes, we looked for a functional impact on iodo-Tg processing, so as to explain TSH feed-back and partial TSH refractoriness. By immunofluorescence, we frequently found iodo-Tg retained in LAMP-1-labeled lysosomes selectively in *Ctns*$^{-/-}$ hypertrophic thyrocytes, suggesting defective prohormone processing (Fig 7Bb-e and Suppl Figure 3). This was never observed in WT thyrocytes. Furthermore, by subcellular fractionation using isopycnic centrifugation combined with western blotting, we demonstrated that *Ctns*$^{-/-}$ thyroid lysosomes were denser and contained more iodo-Tg as compared with WT (Figure 8A and Suppl Figure 5). To examine whether accumulation of iodo-Tg in lysosomes could be due to impaired lysosomal enzymatic machinery, we also looked at the expression and activity of cathepsin B and D. Both cathepsins were actually increased at the mRNA level but cathepsin B activity and cathepsin D protein level were not appreciably affected in *Ctns*$^{-/-}$ thyrocytes. We concluded that TH release from Tg in lysosomes is further impaired in *Ctns*$^{-/-}$ thyrocytes while major cathepsins are preserved, pointing instead to a defect in the lysosomal milieu, likely its redox status.

Discussion

In this study, we report for the first time that C57BL/6 *Ctns*$^{-/-}$ mice recapitulate the earliest and almost obligatory endocrine complication of cystinotic children, namely primary hypothyroidism. Longitudinal study of KO mice thus allowed to delineate the early events of thyroid changes, presumably also occurring in affected children before the end-stage atrophy mostly documented in pathological samples. Two complementary pathogenic mechanisms were found to operate in *Ctns*$^{-/-}$ mice: (i) impaired Tg biosynthesis involving the unfolded protein response to ER stress, and contributing to progressive colloid exhaustion; and (ii) impaired lysosomal iodo-Tg proteolytic processing, thus defective TH release. Adaptation mechanisms include TSH increase, accelerated colloid uptake by macropinocytosis, thyrocyte hyperplasia/hyperthrophy combined with microvascular basket expansion, and accelerated cell turnover/apoptosis.

In 9-months *Ctns*$^{-/-}$ mice, TSH was moderately increased with T_4 and T_3 values remaining normal. Increased TSH induced follicle-autonomous hyperplasia/hypertrophy and microvascular basket expansion but was not associated with significant decrease in global expression of iodoTg synthesis-related genes except Tg itself, nor cathepsins B and D, nor of the thyroid hormone transporter, Mct-8. Thus, primary hypothyroidism was adequately compensated at this age ("subclinical") and originated from a more subtle mechanism. Immunofluorescence proved particularly useful to demonstrate proliferation, apoptosis and microvasculature changes. In the integrated angio-follicular units, capillaries not only serve to passively feed thyrocytes and to collect TH, but also take part in an active, bidirectional paracrine cross-talk that instructs follicular embryological differentiation (54). Furthermore, follicular changes upon iodine deficiency/goitrogenesis are closely associated with increased thyroid blood flow and vascular expansion (55, 56). Thus, expansion of follicular capillaries not only reflects increased tissue demands but can be a useful independent functional marker of follicle activation.

The first key pathogenic finding of this study was activation of the UPR. Newly synthesized Tg accounts for > 50% of normal thyrocyte protein content (57) and can be further increased by TSH (58, 59). "Professional" secre-

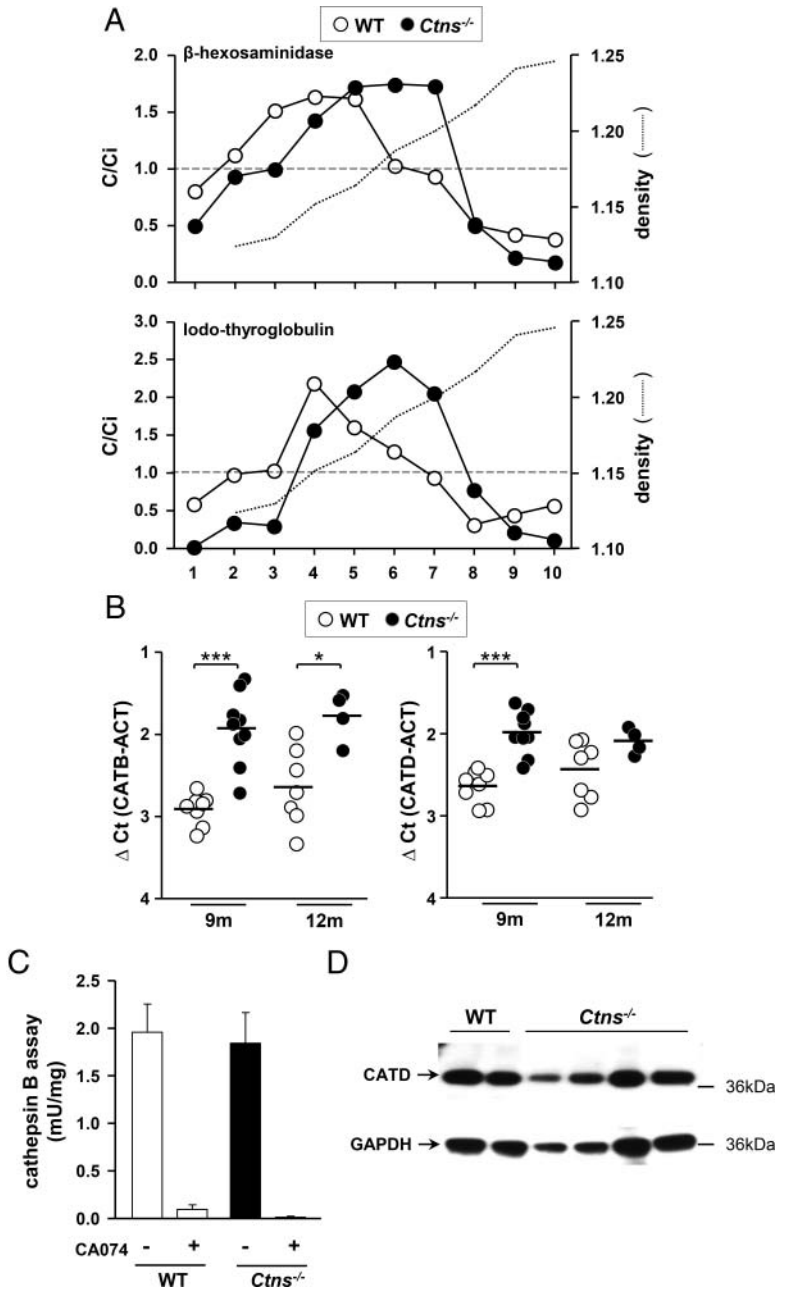

Figure 8. Subcellular fractionation of iodo-thyroglobulin distribution and assessment of hormonogenic cathepsins. A. Sucrose density gradients. Thyroids glands pooled from 4 WT (open symbols) or 4 *Ctns*$^{-/-}$ mice (filled symbols) were homogenized and postnuclear particles were resolved by isopycnic centrifugation into linear sucrose gradients. Ten fractions were collected from the bottom and analyzed for density (dotted lines), β-hexosaminidase activity as lysosomal marker (upper panel), and iodo-Tg (lower panel; densitometry of western blot bands with molecular weight > 250 kDa, ie, the sum of monomer and oligomers). Results are expressed by reference to the sum of all fractions, so that C/Ci indices > 1 indicate enrichment level over initial concentration (broken lines). *Corresponding western blots are shown in Supplemental Figure 5*. In *Ctns*$^{-/-}$ mice, iodo-thyroglobulin accumulates in fractions corresponding to lysosomes, equilibrating at higher density as compared to WT mice. Representative experiment out of two. **B-D. Cathepsins B/D expression and activity are not defective in *Ctns*$^{-/-}$ thyroid glands. B. Expression of cathepsin B and D mRNA.** Quantification by RT-qPCR of cathepsin B (CATB) and cathepsin D (CATD) mRNAs in WT and *Ctns*$^{-/-}$ thyroids collected at 9 and 12 months, normalized to actin (ACT) and presented as ΔCt values. **C. Cathepsin B activity.** Cathepsin B activity, assayed using Z-Phe-Arg-AMC, is given by the difference in absence or presence of the specific inhibitor, CA-074; data normalized to protein concentration. **D. Western blot for Cathepsin D**. Thyroid

tory cells such as thyrocytes have a well-developed pathway for protein export and rely on a sophisticated quality control (QC) machinery to escape ER stress when overstimulated. However, when ER folding capacity is exceeded, or fully abrogated by Tg point mutations (38, 60), UPR is triggered to (i) attenuate protein synthesis, (ii) up-regulate folding capacity and (iii) increase protein degradation by proteasomes. We here demonstrate that Tg accumulates in the dilated ER of *Ctns*$^{-/-}$ thyrocytes, yet with decreased mRNA level despite higher TSH stimulation. Folding of core-glycosylated Tg necessitates the simultaneous assistance of a variety of ER-resident chaperones (eg, GRP78) and foldase (PDI), both of which were strongly increased in *Ctns*$^{-/-}$ thyroids. GRP78 is a major quality-control monitor of Tg folding status (61, 62). Formation of mixed-disulfide folding intermediates between Tg and the ER oxidoreductase, PDI, is crucial for Tg maturation and export (63). These chaperones functionally depend on ER redox homeostasis and high ATP levels, both of which are impaired in cystinosis (51, 64, 65). Combined with general concepts from literature, our data on *Ctns*$^{-/-}$ thyrocytes are thus consistent with the hypotheses that (i) correct Tg disulfide bonding is slower due to impaired luminal redox, which results in misfolded/unfolded Tg accumulation in ER, triggering the UPR response; consequently (ii) slower ER exit / impaired secretion leads to ER dilatation and contributes to colloid exhaustion .

Activation of ER-resident chaperones associated with UPR has been analyzed in detail in a congenital hypothyroidism goiter due to a mutated Tg trafficking defect (38, 66, 67). In contrast, immortalized FRTL5 cells showed increased expression of ER chaperones upon ac-

tivation of Tg synthesis by TSH independently of UPR (no alternative XBP-1 splicing nor CHOP expression) (68). In most 9 and 12 month-old *Ctns*$^{-/-}$ thyroids, we here report the alternative splicing of XBP-1 as well as coordinated increased expression of ATF-4 and CHOP, strongly supporting activation of UPR in response to ER stress. This conclusion has several implications. XBP-1 transcriptional activation triggers ER expansion (69, 70), as we observed in *Ctns*$^{-/-}$ thyrocytes, but also promotes gene transcription of ER resident chaperones (71) and of proteins involved in ER-associated degradation of misfolded/unfolded protein by proteasome (ERAD). Moreover, induced CHOP expression triggers apoptosis, in particular via down-regulation of the major antiapoptotic regulator, Bcl-2 (for a review, see (40)). This mechanism likely contributes to apoptotic thyrocyte shedding, as evidenced by accumulation of cell remnants immunolabeled for cleaved caspase-3 immunolabeling in *Ctns*$^{-/-}$ colloid.

Also consistent with a role for UPR in cystinotic thyroid physiopathology, activation of UPR has been demonstrated in cystinotic proximal tubular cells (37, 51, 72) and in several noncystinotic lysosomal storage diseases (72). Interestingly, rescue of Rab27a-dependent vesicular trafficking alleviated defective lysosomal transport and reduced ER stress in cystinotic proximal tubular cells (37). Rab27a is a Ras-related small GTPase that regulates vesicular transport and exocytosis in a variety of secretory cells, including thyrocytes. We therefore raise the possibility that, in the thyroid gland, lysosomal vesicular transport defect due to cystine overload may be linked to ER stress and UPR activation.

Our second key pathogenic observations in *Ctns*$^{-/-}$ thyrocytes relate to structural and functional endocytic alterations. These include (i) induced macropinocytosis as expected for TSH stimulation; (ii) retention of undigested iodo-Tg in enlarged (LAMP-1-immunolabeling) and denser endosomes/lysosomes (fractionation data), indicating defective Tg lysosomal degradation without alteration of lysosomal cathepsin expression and activity; and (iii) progressive build-up of lysosomal cystine needles and exclusion of cystine-crystal bearing lysosomes from endocytic trafficking. Increases lysosomal density is better accounted for by protein (density, 1.33 g/ml) than cystine crystal accumulation (1.73 g/ml; (73)). Similar alterations in the apical endocytic pathway have recently been demonstrated in *Ctns*$^{-/-}$ kidney proximal tubular cells (PTCs), but lesions appeared earlier on and crystals were more prominent than in thyrocytes (33, 34). Although kidney PTCs and thyrocytes are both specialized for apical endocytosis, the constitutive endocytic rate is faster in PTCs, and the sequence of kidney then thyroid lesions in *Ctns*$^{-/-}$ mice also mimics the order of appearance of clinical signs in cystinotic children (4).

Lysosomal cargo retention despite conservation of hydrolytic equipment implies an altered lysosomal milieu, probably an impaired redox environment as immediate consequence of cystine sequestration. Alteration of intracellular redox potential due to defective lysosomal cystine export has been broadly associated to cystinosis physiopathology (64). Thyroid hormone release from Tg requires stepwise proteolytic processing by synergistic endopeptidases acting at specific sites around conserved N-terminal and C-terminal hormonogenic residues, allowing for final pruning by exopeptidases (23–27). However, the crucial endopeptidases cathepsin B and D were not appreciably affected in *Ctns*$^{-/-}$ thyrocytes. The need for a lysosomal supply of reducing equivalents to expose buried cathepsin-sensitive peptide is supported by the acceleration of Tg degradation by lysosomal proteinases in a reducing environment (22, 74). In vitro, GSH addition boosted degradation of Tg by a thyroid phagolysosome-enriched fraction (22). This effect was originally attributed to substrate unfolding, a conclusion confirmed with highly purified cathepsin D and ^{125}I-thyroglobulin, supporting the concept that Tg unfolding by disulfide bond reduction renders it more susceptible to proteolysis (75). However, a combined effect on activation of cysteine proteinases is now well-accepted (15, 23). A lysosomal cysteine import system has been demonstrated (14) but associated gene(s) remain to be identified. We thus propose that, in *Ctns*$^{-/-}$ thyrocytes, alteration of lysosomal redox status upon cystine accumulation impairs cathepsin action. In turn, defective lysosomal processing of iodo-Tg leads to decreased TH production, thus primary hypothyroidism, eliciting a compensatory TSH response, thyrocyte hypertrophy/hyperplasia and integrated vascular expansion as well as accelerated endocytosis by macropinocytosis.

Endocrine dysfunction related to a lysosomal storage disorder is not unique to cystinosis. Subclinical hypothyroidism with elevated TSH has been reported in patients affected by Fabry disease (lysosomal galactosidase-A deficiency: (76, 77) and Hurler syndrome/mucopolysaccharidosis type IH (α-L-iduronidase deficiency: (78)), which are more frequent than cystinosis. However, to the best of our knowledge, their underlying thyroid physiopathology has not been explored. Comparison of Tg synthesis and processing into TH in corresponding KO mouse models would be interesting.

Legend to Figure 8 Continued. . .
extracts from 2 WT and 4 *Ctns*$^{-/-}$ individual mice at 11–12 months were analyzed by western blotting with antibodies to cathepsin D (CATD), using GAPDH for normalization in parallel blots.

In conclusion, 9-months old C57BL/6 *Ctns*$^{-/-}$ mice recapitulate several key features of infantile cystinosis underlying compensated/subclinical hypothyroidism, namely chronically increased TSH, follicular activation and proliferation and eventual thyrocyte lysosomal crystals. They also disclose early pathogenic, so far unreported mechanisms, such as ER stress triggering UPR, itself contributing to apoptosis; and impaired endolysosomal trafficking associated with defective lysosomal Tg processing. Combination of impaired Tg secretion and accelerated endocytosis provide a satisfactory explanation for colloid exhaustion. We suggest that defective Tg processing following silent accumulation of Tg-derived cystine (single substrate) is the *primum movens* event of the other functional and structural changes. Thus, C57BL/6 *Ctns*$^{-/-}$ mice are a useful model to better understand early pathogenic vs adaptative cascades leading to eventual cystinotic thyroid atrophy; and to evaluate the stage-specific benefit (and limitations) of conventional (cysteamine) or new drugs to be developed, as well as novel therapies such as gene therapy via stem cells (79–81). A particularly promising generic approach for gene therapy, validated in mice, is based on hematopoietic stem cell (HSC) correction, by which immunocompatible grafted cells bearing normal cystinosin (or other) genes are selectively attracted to diseased tissue areas. We recently reported that HSCs project expansions, known as tunneling nanotubes, whereby they physically interconnect with diseased epithelial cells across basement laminae, and can bidirectionally exchange lysosomes by tubulin-based motion (82).

Acknowledgments

This work was mainly supported by the Cystinosis Research Foundation, Belgian Science Policy Office-Interuniversity Attraction Poles program IAP P7/43-BeMGI, Belgian Fonds de la Recherche Scientifique (F.R.S-FNRS) and Actions de Recherche concertées (to CEP and PJC), National Institutes of Health RO1-DK090058, R21-DK090548 and RO1-DK099338 (to SC). This work was also supported in part by Grants R37-DK15070 from the National Institutes of Health (to SR). The content is solely the responsibility of the authors and does not necessarily represent the official NIH views. The Platform for Imaging Cells and Tissues (PICT) was financed by National Lottery, Région bruxelloise, Région wallonne, Université catholique de Louvain and de Duve Institute (to PC). HGC is Postdoctoral Researcher and CEP is Senior Research Associate at F.R.S-FNRS (Belgium). We thank Dr. E. Marbaix for helpful advice in thyroid pathology, Dr. T. Arnould for valuable suggestions on endoplasmic reticulum stress, Dr. Ris-Stalpers for providing anti-iodo-Tg antibodies and Mrs L. Thanh for assistance with EM.

Address all correspondence and requests for reprints to: Héloïse P. Gaide Chevronnay, PhD, de Duve Institute and Université catholique de Louvain, 75, avenue Hippocrate, PO Box B1.75.05, 1200-Brussels, Belgium, Phone +32 2 764.75.55, FAX +32 2 764.75.41, e-mail : heloise.gaidechevronnay@uclouvain.be.

Disclosure Summary: The authors have nothing to disclose
This work was supported by .

References

1. **Van Vliet G.** Development of the thyroid gland: lessons from congenitally hypothyroid mice and men. *Clinical genetics*. 2003;63(6):445–455.
2. **Grasberger H, Refetoff S. Congenital defects of thyroid hormone synthesis. In: Weiss RE, Refetoff S.** eds. *Genetics Diagnosis of Endocrine Disorders*. Amsterdam, The Netherlands: Academic Press, Elsevier, Inc.;2010:87–95.
3. **Gahl WA, Thoene JG, Schneider JA.** Cystinosis. *The New England journal of medicine*. 2002;347(2):111–121.
4. **Gahl WA, Thoene J.** Cystinosis: A Disorder of Lysosomal Membrane Transport. In: Scriver CR, Beaudet AL, Sly WS, Valle D, Childs B, Kinzler KW, Vogelstein B, eds. *The Metabolic and Molecular Basis of Inherited Disease*. Vol 3. Eight Edition ed: McGraw-Hill Companies, Inc.;2001: 5085–5108. *Online update 2013*.
5. **Chan AM, Lynch MJ, Bailey JD, Ezrin C, Fraser D.** Hypothyroidism in cystinosis. A clinical, endocrinologic and histologic study involving sixteen patients with cystinosis. *The American journal of medicine*. 1970;48(6):678–692.
6. **Broyer M, Niaudet P.** Cystinosis. In: Saudubray JM, van den Berghe G, Walter JH, eds. *Inborn Metabolic Diseases*: Springer Berlin Heidelberg;2012:617–624.
7. **Cherqui S, Kalatzis V, Trugnan G, Antignac C.** The targeting of cystinosin to the lysosomal membrane requires a tyrosine-based signal and a novel sorting motif. *The Journal of biological chemistry*. 2001;276(16):13314–13321.
8. **Kalatzis V, Cherqui S, Antignac C, Gasnier B.** Cystinosin, the protein defective in cystinosis, is a H(+)-driven lysosomal cystine transporter. *The EMBO journal*. 2001;20(21):5940–5949.
9. **Jezegou A, Llinares E, Anne C, Kieffer-Jaquinod S, O'Regan S, Aupetit J, Chabli A, Sagne C, Debacker C, Chadefaux-Vekemans B, Journet A, Andre B, Gasnier B.** Heptahelical protein PQLC2 is a lysosomal cationic amino acid exporter underlying the action of cysteamine in cystinosis therapy. *Proceedings of the National Academy of Sciences of the United States of America*. 2012;109(50):E3434–3443.
10. **Lucky AW, Howley PM, Megyesi K, Spielberg SP, Schulman JD.** Endocrine studies in cystinosis: compensated primary hypothyroidism. *The Journal of pediatrics*. 1977;91(2):204–210.
11. **Kimonis VE, Troendle J, Rose SR, Yang ML, Markello TC, Gahl WA.** Effects of early cysteamine therapy on thyroid function and growth in nephropathic cystinosis. *The Journal of clinical endocrinology and metabolism*. 1995;80(11):3257–3261.
12. **Brodin-Sartorius A, Tete MJ, Niaudet P, Antignac C, Guest G, Ottolenghi C, Charbit M, Moyse D, Legendre C, Lesavre P, Cochat P, Servais A.** Cysteamine therapy delays the progression of nephropathic cystinosis in late adolescents and adults. *Kidney international*. 2012;81(2):179–189.
13. **Emma F, Nesterova G, Langman C, Labbe A, Cherqui S, Goodyer P, Janssen MC, Greco M, Topaloglu R, Elenberg E, Dohil R, Trauner D, Antignac C, Cochat P, Kaskel F, Servais A, Wuhl E, Niaudet P, Van't Hoff W, Gahl W, Levtchenko E.** Nephropathic cystinosis: an international consensus document. *Nephrology, di-*

alysis, transplantation : official publication of the European Dialysis and Transplant Association - European Renal Association. 2014;29 Suppl 4:iv87–94.
14. **Pisoni RL, Acker TL, Lisowski KM, Lemons RM, Thoene JG.** A cysteine-specific lysosomal transport system provides a major route for the delivery of thiol to human fibroblast lysosomes: possible role in supporting lysosomal proteolysis. *The Journal of cell biology*. 1990;110(2):327–335.
15. **Brix K, Lemansky P, Herzog V.** Evidence for extracellularly acting cathepsins mediating thyroid hormone liberation in thyroid epithelial cells. *Endocrinology*. 1996;137(5):1963–1974.
16. **Friedrichs B, Tepel C, Reinheckel T, Deussing J, von Figura K, Herzog V, Peters C, Saftig P, Brix K.** Thyroid functions of mouse cathepsins B, K, and L. *The Journal of clinical investigation*. 2003; 111(11):1733–1745.
17. **Edelhoch H, Rall J.** The proteins and enzymes of the thyroid In: Pitt-Rivers R, Trotter W, eds. *The Thyroid Gland* London: Butterworths 1964:113–130.
18. **Herzog V, Berndorfer U, Saber Y.** Isolation of insoluble secretory product from bovine thyroid: extracellular storage of thyroglobulin in covalently cross-linked form. *The Journal of cell biology*. 1992; 118(5):1071–1083.
19. **Gerard AC, Denef JF, Colin IM, van den Hove MF.** Evidence for processing of compact insoluble thyroglobulin globules in relation with follicular cell functional activity in the human and the mouse thyroid. *European journal of endocrinology / European Federation of Endocrine Societies*. 2004;150(1):73–80.
20. **Klein M, Gestmann I, Berndorfer U, Schmitz A, Herzog V.** The thioredoxin boxes of thyroglobulin: possible implications for intermolecular disulfide bond formation in the follicle lumen. *Biological chemistry*. 2000;381(7):593–601.
21. **Berndorfer U, Wilms H, Herzog V.** Multimerization of thyroglobulin (TG) during extracellular storage: isolation of highly cross-linked TG from human thyroids. *The Journal of clinical endocrinology and metabolism*. 1996;81(5):1918–1926.
22. **Peake BL, Balasubramaniam K, Deiss WP.** Effect of reduced glutathione on the proteolysis of intraparticulate and native thyroglobulin. *Biochimica and biophysica acta*. 1967;148:689–702.
23. **Yoshinari M, Taurog A.** Lysosomal digestion of thyroglobulin: role of cathepsin D and thiol proteases. *Endocrinology*. 1985;117(4): 1621–1631.
24. **Dunn AD, Dunn JT.** Cysteine proteinases from human thyroids and their actions on thyroglobulin. *Endocrinology*. 1988;123(2):1089–1097.
25. **Dunn AD, Crutchfield HE, Dunn JT.** Proteolytic processing of thyroglobulin by extracts of thyroid lysosomes. *Endocrinology*. 1991; 128(6):3073–3080.
26. **Dunn AD, Myers HE, Dunn JT.** The combined action of two thyroidal proteases releases T4 from the dominant hormone-forming site of thyroglobulin. *Endocrinology*. 1996;137(8):3279–3285.
27. **Nakagawa H, Ohtaki S.** Thyroxine (T4) release from thyroglobulin and its T4-containing peptide by thyroid thiol proteases. *Endocrinology*. 1985;116(4):1433–1439.
28. **Marino M, McCluskey RT.** Role of thyroglobulin endocytic pathways in the control of thyroid hormone release. *American journal of physiology Cell physiology*. 2000;279(5):C1295–1306.
29. **Croizet-Berger K, Daumerie C, Couvreur M, Courtoy PJ, van den Hove MF.** The endocytic catalysts, Rab5a and Rab7, are tandem regulators of thyroid hormone production. *Proceedings of the National Academy of Sciences of the United States of America*. 2002; 99(12):8277–8282.
30. **van den Hove MF, Croizet-Berger K, Tyteca D, Selvais C, de Diesbach P, Courtoy PJ.** Thyrotropin activates guanosine 5′-diphosphate/guanosine 5′-triphosphate exchange on the rate-limiting endocytic catalyst, Rab5a, in human thyrocytes in vivo and in vitro. *The Journal of clinical endocrinology and metabolism*. 2007;92(7): 2803–2810.
31. **Fujita H.** Functional morphology of the thyroid. *International review of cytology*. 1988;113:145–185.
32. **Di Cosmo C, Liao XH, Dumitrescu AM, Philp NJ, Weiss RE, Refetoff S.** Mice deficient in MCT8 reveal a mechanism regulating thyroid hormone secretion. *The Journal of clinical investigation*. 2010; 120(9):3377–3388.
33. **Gaide Chevronnay HP, Janssens V, Van Der Smissen P, N′Kuli F, Nevo N, Guiot Y, Levtchenko E, Marbaix E, Pierreux CE, Cherqui S, Antignac C, Courtoy PJ.** Time course of pathogenic and adaptation mechanisms in cystinotic mouse kidneys. *Journal of the American Society of Nephrology : JASN*. 2014;25(6):1256–1269.
34. **Raggi C, Luciani A, Nevo N, Antignac C, Terryn S, Devuyst O.** Dedifferentiation and aberrations of the endolysosomal compartment characterize the early stage of nephropathic cystinosis. *Human molecular genetics*. 2014.
35. **Cherqui S, Sevin C, Hamard G, Kalatzis V, Sich M, Pequignot MO, Gogat K, Abitbol M, Broyer M, Gubler MC, Antignac C.** Intralysosomal cystine accumulation in mice lacking cystinosin, the protein defective in cystinosis. *Molecular and cellular biology*. 2002;22(21): 7622–7632.
36. **Nevo N, Chol M, Bailleux A, Kalatzis V, Morisset L, Devuyst O, Gubler MC, Antignac C.** Renal phenotype of the cystinosis mouse model is dependent upon genetic background. *Nephrology, dialysis, transplantation : official publication of the European Dialysis and Transplant Association - European Renal Association*. 2010;25(4): 1059–1066.
37. **Johnson JL, Napolitano G, Monfregola J, Rocca CJ, Cherqui S, Catz SD.** Upregulation of the Rab27a-dependent trafficking and secretory mechanisms improves lysosomal transport, alleviates endoplasmic reticulum stress, and reduces lysosome overload in cystinosis. *Molecular and cellular biology*. 2013;33(15):2950–2962.
38. **Baryshev M, Sargsyan E, Wallin G, Lejnieks A, Furudate S, Hishinuma A, Mkrtchian S.** Unfolded protein response is involved in the pathology of human congenital hypothyroid goiter and rat nongoitrous congenital hypothyroidism. *Journal of molecular endocrinology*. 2004;32(3):903–920.
39. **Hetz C.** The unfolded protein response: controlling cell fate decisions under ER stress and beyond. *Nature reviews Molecular cell biology*. 2012;13(2):89–102.
40. **Szegezdi E, Logue SE, Gorman AM, Samali A.** Mediators of endoplasmic reticulum stress-induced apoptosis. *EMBO reports*. 2006; 7(9):880–885.
41. **Pohlenz J, Maqueem A, Cua K, Weiss RE, Van Sande J, Refetoff S.** Improved radioimmunoassay for measurement of mouse thyrotropin in serum: strain differences in thyrotropin concentration and thyrotroph sensitivity to thyroid hormone. *Thyroid : official journal of the American Thyroid Association*. 1999;9(12):1265–1271.
42. **Pierreux CE, Cordi S, Hick AC, Achouri Y, Ruiz de Almodovar C, Prevot PP, Courtoy PJ, Carmeliet P, Lemaigre FP.** Epithelial: Endothelial cross-talk regulates exocrine differentiation in developing pancreas. *Developmental biology*. 2010;347(1):216–227.
43. **Gaide Chevronnay HP, Cornet PB, Delvaux D, Lemoine P, Courtoy PJ, Henriet P, Marbaix E.** Opposite regulation of transforming growth factors-beta2 and -beta3 expression in the human endometrium. *Endocrinology*. 2008;149(3):1015–1025.
44. **Zachara NE, Vosseller K, Hart GW.** Detection and analysis of proteins modified by O-linked N-acetylglucosamine. *Current protocols in protein science / editorial board, John E Coligan* [*et al*]. 2011; Chapter 12:Unit12 18.
45. **Barrett AJ.** Fluorimetric assays for cathepsin B and cathepsin H with methylcoumarylamide substrates. *The Biochemical journal*. 1980; 187(3):909–912.
46. **Colin IM, Denef JF, Lengele B, Many MC, Gerard AC.** Recent insights into the cell biology of thyroid angiofollicular units. *Endocrine reviews*. 2013;34(2):209–238.
47. **Coclet J, Foureau F, Ketelbant P, Galand P, Dumont JE.** Cell pop-

ulation kinetics in dog and human adult thyroid. *Clinical endocrinology*. 1989;31(6):655–665.
48. **Park MA, Thoene JG.** Potential role of apoptosis in development of the cystinotic phenotype. *Pediatric nephrology*. 2005;20(4):441–446.
49. **Sansanwal P, Kambham N, Sarwal MM.** Caspase-4 may play a role in loss of proximal tubules and renal injury in nephropathic cystinosis. *Pediatric nephrology*. 2010;25(1):105–109.
50. **Leonardi A, Vito P, Mauro C, Pacifico F, Ulianich L, Consiglio E, Formisano S, Di Jeso B.** Endoplasmic reticulum stress causes thyroglobulin retention in this organelle and triggers activation of nuclear factor-kappa B via tumor necrosis factor receptor-associated factor 2. *Endocrinology*. 2002;143(6):2169–2177.
51. **Sansanwal P, Li L, Hsieh SC, Sarwal MM.** Insights into novel cellular injury mechanisms by gene expression profiling in nephropathic cystinosis. *Journal of inherited metabolic disease*. 2010;33(6):775–786.
52. **Oslowski CM, Urano F.** Measuring ER stress and the unfolded protein response using mammalian tissue culture system. *Methods in enzymology*. 2011;490:71–92.
53. **Samali A, Fitzgerald U, Deegan S, Gupta S.** Methods for monitoring endoplasmic reticulum stress and the unfolded protein response. *International journal of cell biology*. 2010;2010:830307.
54. **Hick AC, Delmarcelle AS, Bouquet M, Klotz S, Copetti T, Forez C, Van Der Smissen P, Sonveaux P, Collet JF, Feron O, Courtoy PJ, Pierreux CE.** Reciprocal epithelial:endothelial paracrine interactions during thyroid development govern follicular organization and C-cells differentiation. *Developmental biology*. 2013;381(1):227–240.
55. **Ramsden JD, Buchanan MA, Egginton S, Watkinson JC, Mautner V, Eggo MC.** Complete inhibition of goiter in mice requires combined gene therapy modification of angiopoietin, vascular endothelial growth factor, and fibroblast growth factor signaling. *Endocrinology*. 2005;146(7):2895–2902.
56. **Imada M, Kurosumi M, Fujita H.** Three-dimensional aspects of blood vessels in thyroids from normal, low iodine diet-treated, TSH-treated, and PTU-treated rats. *Cell and tissue research*. 1986;245(2):291–296.
57. **Van Herle AJ, Vassart G, Dumont JE.** Control of thyroglobulin synthesis and secretion. (First of two parts). *The New England journal of medicine*. 1979;301(5):239–249.
58. **Van Heuverswyn B, Streydio C, Brocas H, Refetoff S, Dumont J, Vassart G.** Thyrotropin controls transcription of the thyroglobulin gene. *Proceedings of the National Academy of Sciences of the United States of America*. 1984;81(19):5941–5945.
59. **Van Heuverswyn B, Leriche A, Van Sande J, Dumont JE, Vassart G.** Transcriptional control of thyroglobulin gene expression by cyclic AMP. *FEBS letters*. 1985;188(2):192–196.
60. **Kim PS, Lee J, Jongsamak P, Menon S, Li B, Hossain SA, Bae JH, Panijpan B, Arvan P.** Defective protein folding and intracellular retention of thyroglobulin-R19K mutant as a cause of human congenital goiter. *Molecular endocrinology*. 2008;22(2):477–484.
61. **Kim PS, Bole D, Arvan P.** Transient aggregation of nascent thyroglobulin in the endoplasmic reticulum: relationship to the molecular chaperone, BiP. *The Journal of cell biology*. 1992;118(3):541–549.
62. **Kim PS, Arvan P.** Calnexin and BiP act as sequential molecular chaperones during thyroglobulin folding in the endoplasmic reticulum. *The Journal of cell biology*. 1995;128(1–2):29–38.
63. **Di Jeso B, Park YN, Ulianich L, Treglia AS, Urbanas ML, High S, Arvan P.** Mixed-disulfide folding intermediates between thyroglobulin and endoplasmic reticulum resident oxidoreductases ERp57 and protein disulfide isomerase. *Molecular and cellular biology*. 2005;25(22):9793–9805.
64. **Levtchenko E, de Graaf-Hess A, Wilmer M, van den Heuvel L, Monnens L, Blom H.** Altered status of glutathione and its metabolites in cystinotic cells. *Nephrology, dialysis, transplantation : official publication of the European Dialysis and Transplant Association - European Renal Association*. 2005;20(9):1828–1832.
65. **Levtchenko EN, Wilmer MJ, Janssen AJ, Koenderink JB, Visch HJ, Willems PH, de Graaf-Hess A, Blom HJ, van den Heuvel LP, Monnens LA.** Decreased intracellular ATP content and intact mitochondrial energy generating capacity in human cystinotic fibroblasts. *Pediatric research*. 2006;59(2):287–292.
66. **Medeiros-Neto G, Kim PS, Yoo SE, Vono J, Targovnik HM, Camargo R, Hossain SA, Arvan P.** Congenital hypothyroid goiter with deficient thyroglobulin. Identification of an endoplasmic reticulum storage disease with induction of molecular chaperones. *The Journal of clinical investigation*. 1996;98(12):2838–2844.
67. **Kim PS, Kwon OY, Arvan P.** An endoplasmic reticulum storage disease causing congenital goiter with hypothyroidism. *The Journal of cell biology*. 1996;133(3):517–527.
68. **Christis C, Fullaondo A, Schildknegt D, Mkrtchian S, Heck AJ, Braakman I.** Regulated increase in folding capacity prevents unfolded protein stress in the ER. *Journal of cell science*. 2010;123(Pt 5):787–794.
69. **Sriburi R, Jackowski S, Mori K, Brewer JW.** XBP1: a link between the unfolded protein response, lipid biosynthesis, and biogenesis of the endoplasmic reticulum. *The Journal of cell biology*. 2004;167(1):35–41.
70. **Shaffer AL, Shapiro-Shelef M, Iwakoshi NN, Lee AH, Qian SB, Zhao H, Yu X, Yang L, Tan BK, Rosenwald A, Hurt EM, Petroulakis E, Sonenberg N, Yewdell JW, Calame K, Glimcher LH, Staudt LM.** XBP1, downstream of Blimp-1, expands the secretory apparatus and other organelles, and increases protein synthesis in plasma cell differentiation. *Immunity*. 2004;21(1):81–93.
71. **Lee AH, Iwakoshi NN, Glimcher LH.** XBP-1 regulates a subset of endoplasmic reticulum resident chaperone genes in the unfolded protein response. *Molecular and cellular biology*. 2003;23(21):7448–7459.
72. **Wei H, Kim SJ, Zhang Z, Tsai PC, Wisniewski KE, Mukherjee AB.** ER and oxidative stresses are common mediators of apoptosis in both neurodegenerative and non-neurodegenerative lysosomal storage disorders and are alleviated by chemical chaperones. *Human molecular genetics*. 2008;17(4):469–477.
73. **Schulman JD, Bradley KH, Seegmiller JE.** Cystine: compartmentalization within lysosomes in cystinotic leukocytes. *Science*. 1969;166(3909):1152–1154.
74. **Pisarev MA, Dumont JE.** The role of reduced glutathione in thyroglobulin proteolysis iv vitro. *Acta endocrinologica*. 1975;79(1):76–85.
75. **Dunn AD, Dunn JT.** Thyroglobulin degradation by thyroidal proteases: action of purified cathepsin D. *Endocrinology*. 1982;111(1):280–289.
76. **Faggiano A, Pisani A, Milone F, Gaccione M, Filippella M, Santoro A, Vallone G, Tortora F, Sabbatini M, Spinelli L, Lombardi G, Cianciaruso B, Colao A.** Endocrine dysfunction in patients with Fabry disease. *The Journal of clinical endocrinology and metabolism*. 2006;91(11):4319–4325.
77. **Hauser AC, Gessl A, Lorenz M, Voigtlander T, Fodinger M, Sunder-Plassmann G.** High prevalence of subclinical hypothyroidism in patients with Anderson-Fabry disease. *Journal of inherited metabolic disease*. 2005;28(5):715–722.
78. **Polgreen LE, Tolar J, Plog M, Himes JH, Orchard PJ, Whitley CB, Miller BS, Petryk A.** Growth and endocrine function in patients with Hurler syndrome after hematopoietic stem cell transplantation. *Bone marrow transplantation*. 2008;41(12):1005–1011.
79. **Syres K, Harrison F, Tadlock M, Jester JV, Simpson J, Roy S, Salomon DR, Cherqui S.** Successful treatment of the murine model of cystinosis using bone marrow cell transplantation. *Blood*. 2009;114(12):2542–2552.
80. **Yeagy BA, Harrison F, Gubler MC, Koziol JA, Salomon DR, Cherqui S.** Kidney preservation by bone marrow cell transplantation in

hereditary nephropathy. *Kidney international*. 2011;79(11):1198–1206.
81. **Harrison F, Yeagy BA, Rocca CJ, Kohn DB, Salomon DR, Cherqui S.** Hematopoietic stem cell gene therapy for the multisystemic lysosomal storage disorder cystinosis. *Molecular therapy : the journal of the American Society of Gene Therapy*. 2013;21(2):433–444.
82. **Naphade S, Sharma J, Gaide Chevronnay HP, Shook MA, Yeagy BA, Rocca CJ, Ur SN, Lau AJ, Courtoy PJ, Cherqui S.** Brief reports: Lysosomal cross-correction by hematopoietic stem cell-derived macrophages via tunneling nanotubes. *Stem cells*. 2015;33(1):301–309.